Synergistic use of Lagrangian dispersion and radiative transfer modelling, and satellite and surface remote sensing measurements for the investigation of volcanic plumes: the Mount Etna eruption of 25–27 October 2013

P. Sellitto[1], **A. di Sarra**[2], **S. Corradini**[3], **M. Boichu**[1,4], **H. Herbin**[4], **P. Dubuisson**[4], **G. Sèze**[1], **D. Meloni**[2], **F. Monteleone**[5], **L. Merucci**[3], **J. Rusalem**[4], **G. Salerno**[6], **P. Briole**[7], and **B. Legras**[1]

[1]Laboratoire de Météorologie Dynamique, UMR8539, CNRS – École Normale Supérieure/Université Pierre et Marie Curie/Ecole Polytechnique, Paris, France
[2]ENEA, Laboratory for Observations and Analyses of the Earth and Climate (SSPT-PROTER-OAC), Rome, Italy
[3]Istituto Nazionale di Geofisica e Vulcanologia, Rome, Italy
[4]Laboratoire d'Optique Atmosphérique, UMR8518, CNRS – Université de Lille 1, Villeneuve d'Ascq, France
[5]ENEA, UTMEA-TER, Palermo, Italy
[6]Istituto Nazionale di Geofisica e Vulcanologia, Catania, Italy
[7]Laboratoire de Géologie, UMR8538, CNRS - École Normale Supérieure, Paris, France

Correspondence to: P. Sellitto (psellitto@lmd.ens.fr)

1

Abstract

In this paper we combine SO_2 and ash plume dispersion modelling, satellite and surface remote sensing observations to study the regional influence of a relatively weak volcanic eruption from Mount Etna on the optical and micro-physical properties of Mediterranean
5　aerosols. We analyse the Mount Etna eruption episode of 25–27 October 2013. The evolution of the plume along the trajectory is investigated by means of the FLEXible PARTicle Lagrangian dispersion (FLEXPART) model. The satellite dataset includes true colour images, retrieved values of volcanic SO_2 and ash, and estimates of SO_2 and ash emission rates derived from MODIS (MODerate resolution Imaging Spectroradiometer) observations,
10　and estimates of cloud top pressure from SEVIRI (Spinning Enhanced Visible and InfraRed Imager). Surface remote sensing measurements of aerosol and SO_2 made at the ENEA Station for Climate Observations (35.52° N, 12.63° E, 50 m a.s.l.) on the island of Lampedusa are used in the analysis. The combination of these different datasets suggests that SO_2 and ash, despite the initial injection at about 7.0 km altitude, reached altitudes around
15　10–12 km and influenced the column average aerosol particle size distribution at a distance of more than 350 km downwind. This study indicates that even a relatively weak volcanic eruption may produce an observable effect on the aerosol properties at the regional scale. The impact of secondary sulphate particles on the aerosol size distribution at Lampedusa is discussed, and estimates of the clear sky direct aerosol radiative forcing are derived. Daily
20　shortwave radiative forcing efficiencies, i.e. radiative forcing per unit AOD (Aerosol Optical Depth), are calculated with the LibRadtran model. They are estimated between -39 and -48 W m^{-2} AOD^{-1} at the top of the atmosphere, and between -66 and -49 W m^{-2} AOD^{-1}, at the surface, with the variability in the estimates mainly depending on the aerosol single scattering albedo. These results suggest that sulphate particles played a large role
25　in the transported plume composition and radiative forcing, while the contribution by ash particles was small in the volcanic plume arriving at Lampedusa during this event.

1 Introduction

Volcanic eruptions influence tropospheric and stratospheric composition (see, e.g., von Glasow et al., 2009), the Earth's radiation budget from the regional to the global scale, and the Earth's climate (see, e.g., Robock and Oppenheimer, 2003). Strong explosive eruptions
5 have been observed to produce a cooling of the Earth, primarily due to long-lived highly reflecting stratospheric sulphate aerosols and their influence on the radiative budget (Mc-Cormick et al., 1995; Hamill et al., 1997; SPARC, 2006). While the impact of the strong explosive eruptions reaching the stratosphere is relatively well known, the influence of the more frequent weak volcanic activity on the tropospheric aerosol properties and on the
10 radiation transfer is still largely unknown (Oppenheimer et al., 2011).

A number of studies show that moderate volcanic eruptions may potentially affect tropospheric composition and air quality (see, e.g., Satsumabayashi et al., 2004; Colette et al., 2011). They may also impact aerosol (see, e.g., Huebert et al., 2001; Waquet et al., 2014) and cloud properties (see, e.g., Gassó, 2008), and affect the regional radiation budget (see,
15 e.g., Flanner et al., 2014), also at relatively distant locations and for relatively long time periods. These effects depend on emission strength, injection altitude, life cycle of the different compounds, and local and regional dynamics. Most of the radiative effects of moderate eruptions are associated with changes in the aerosol particle size distribution, composition, and shape. Emission of primary particles, mainly ash, and secondary aerosols, mainly
20 through gas-to-particle conversion of SO_2, affect the aerosol properties.

The formation of sulphate aerosol and its life cycle in the troposphere, in particular, are among the main unknown atmospheric processes. The emitted sulphur dioxide oxidizes to gaseous sulphuric acid, which, in the presence of water vapour and neutralising species, can nucleate and then coagulate and grow, to form liquid droplets of aqueous solutions
25 containing variable amounts of sulphuric acid (von Glasow et al., 2009). How nucleation is initiated at the molecular scale, especially in the volcanic plume conditions (e.g., elevated concentrations of water vapour, which is thought to be a key parameter in nucleation, Vehkamäki et al., 2002) is still largely unknown (Andreae, 2013; Kulmala et al., 2013). The

3

gas-to-particle conversion can occur within very different time-scales (see, e.g., Oppenheimer et al., 1998). The sulphate aerosol lifetime can largely vary, from few a days in the lower troposphere to a few months in the upper troposphere (Stevenson et al., 2003). The regional effect of moderate tropospheric eruptions on the radiation transfer is consequently not well characterised. In addition, present climate models are not able to simulate the overall effect of this relatively weak volcanic activity. Although quiescent degassing and moderate eruptions produce non-negligible effects (Graf et al., 1997), very few studies investigate their impact at the global scale (Santer et al., 2014; Schmidt et al., 2014). A better understanding of the impact of small eruptions on the optical and micro-physical aerosol properties is needed to bridge the relatively weak volcanic activity to their impact at the regional to global scale

In the context of its quasi-continuous relatively weak volcanic activity, Mount Etna, due to its high-degassing-rate alkalinic basalt magma (Gerlach, 1991), stands as a significant emitter of volatile sulphur compounds, estimated to be $0.7 \times 10^6 \, \text{Mg}$ (sulphur) yr^{-1} (Allard et al., 1991). This value is about ten times larger than the anthropogenic sulphur emissions in the Mediterranean area (Graf et al., 1997). Etna is thus an important source of particles and gases for the Mediterranean atmosphere.

A large effort is dedicated by the international community to the understanding of the atmospheric composition and aerosol in the Mediterranean, and their effects on climate. In particular, a large activity is being carried out on these topics within ChArMEx (the Chemistry-Aerosol Mediterranean Experiment; http://charmex.lsce.ipsl.fr/). As part of ChArMEx, a large measurement campaign took place in the western and central Mediterranean in summer 2013 (Mallet et al., 2016), and an extended observation period (EOP) took place from 2011 to 2013. This study contributes to the objectives of ChArMEX by investigating the role played by frequent moderate emissions from Etna on the aerosol composition and the radiation transfer at the regional scale. The event analysed in this study occurred within the ChArMEx EOP, and its characterization helps the understanding of the contribution of different sources and different aerosol types to the aerosols in the Mediterranean region.

4

The impact of volcanic emissions on the tropospheric aerosol properties at the regional scale can be investigated using satellite observations, which also allow, thanks to their spatial coverage, to follow the plume evolution. However, satellite measurements usually have a limited sensitivity to aerosols and their precursors, e.g., sulphur dioxide (e.g. Karagulian et al., 2010). In addition, they provide little detailed information on crucial parameters, e.g., on the SO_2 vertical distribution (e.g. Carboni et al., 2016) and on the ash size distribution(e.g. Stohl et al., 2011). For relatively weak volcanic activity, aerosol and SO_2 amounts are often close to or below the detection limit of instruments onboard satellites. Modelling tools can supply further information, provided that input parameters are carefully selected. Unfortunately, many processes (e.g., dynamical, chemical, micro-physical processes) are still characterised by a poor fundamental knowledge. More detailed information on the downwind impact can be provided by ground-based instruments at selected locations, but, in this case, a limited information on the transport and evolution of the emitted gases and particles is available.

Thus, a reasonable approach consists in exploiting the synergy of observations and simulations of the dynamical, chemical, and micro-physical evolution of the plumes. This approach may be particularly useful to study the effects of relatively weak non-explosive volcanic activity. The downwind impact of volcanic activity can be monitored by ground-based stations, depending on the dynamics of the plume. Efforts for the synergistic use of satellite observations with ground-based measurements and/or modelling have been recently proposed (Webley et al., 2012; McCormick et al., 2014).

In this paper, we apply this synergistic approach to study the moderate eruption of Mount Etna that occurred on 25–27 October 2013. We show how this approach allows a more complete characterization of such a kind of eruptive event, from emissions to downwind impact. We exploit the information coming from different observation and modelling sources: (a) quantitative information on the emissions, obtained from satellite observations, (b) information on the volcanic plume horizontal and vertical dispersion, obtained by a combination of satellite observations and Lagrangian modelling, and (c) information on the downwind time-dependent modifications of the aerosol optical and micro-physical properties,

5

obtained by surface remote sensing observations at the island of Lampedusa. Lampedusa was downwind the plume for this event, due to the prevailing dynamics, and at a relatively large distance (about 350 km).

The paper is organised as follows. In Sect. 2 we introduce the instruments, the data and
5 the methods used in our work. In Sect. 3 we give a qualitative description of the eruption event under investigation. In Sects. 4 and 5 we characterize the sulphur dioxide and ash plume and their dispersions. In Sect. 6 we show and discuss the remote sensing observations at the ground station of Lampedusa, one of the supersites of the ChArMEx experiment. In Sect. 7 we propose a range of variability of the clear sky direct radiative forcing of the
10 aerosol plume, depending on its optical properties and vertical distribution. In Sect. 8 we give conclusions.

2 Methods

2.1 Synergistic use of the different information layers

The different modelling and observational methods described in Sect. 2 are used together
15 to provide a comprehensive description of the eruptive event under investigation. In addition, different synergies are exploited, e.g., the input information needed for one method is obtained from the output of a different method, or different information layers are concurrently used to obtain a clearer picture of the certain processes when a complete view cannot be obtained with one method alone. A scheme of these contributions and synergies
20 is provided in Fig. 1. These contributions and synergies are listed from a) to h), and then referenced throughout the text.

It is worth noting that, for a more complete understanding of the downwind impact of volcanic emissions, two important information layers would be the ones describing the spatial distributions (satellite observations) and the formation/evolution processes
25 (chemistry/micro-physics modelling) of the sulphate aerosols produced by the gas-to-

6

particle conversion of volcanic SO_2 emissions. Work is ongoing to provide these further information layers for future studies.

2.2 Satellite data

2.2.1 Sulphur dioxide retrieval and SO_2/ash emissions rate inversion by MODIS TIR data

The MODerate resolution Imaging Spectroradiometer (MODIS) is a multi-spectral instrument onboard both the NASA (National Aeronautics and Space Administration) Terra and Aqua polar satellites (http://modis.gsfc.nasa.gov/). The MODIS instrument has 36 spectral bands from the VISible (VIS) to the Thermal InfraRed (TIR), a swath width of 2330 km and a repetition cycle of 1 or 2 days. The spatial resolution in the TIR channels used for the sulphur dioxide total column retrieval is $1 km \times 1 km$.

The SO_2 total column retrieval by MODIS is based on the SO_2 wide absorption around 8.6 μm (MODIS channel 29). The retrieval scheme used in this study is based on the Volcanic Plume Removal (VPR) approach developed for the Etna volcano (Pugnaghi et al., 2013). The VPR procedure also takes into account the ash influence on SO_2 estimates by using the channels centred around 11 and 12 μm (MODIS channels 31 and 32) (Corradini et al., 2009). Volcanic cloud top altitude and temperature are needed as input in the retrieval scheme. The cloud top temperature has been assumed to correspond to the brightness temperature of the volcanic plume most opaque pixel (Prata and Grant, 2001; Corradini et al., 2010). The cloud top altitude was obtained by comparing the brightness temperature with the atmospheric temperature profile measured from the WMO (World Meteorological Organization) meteorological station based in Trapani (about 200 km West of Mount Etna, $37.92° N$, $12.50° E$), on the same day of the MODIS measurements at approximately the same time (radio-sounding of 26 October at 12:00 UTC; hereafter, all times reported are in UTC).

A single satellite image contains the signature of volcanic emissions at a specific time. The SO_2 and ash emission rates at vents can be reconstructed by defining a volcanic plume

axis, along the plume, and transects, perpendicular to the axis, on the SO_2 and ash (this latter not shown here) retrieval maps. The emission rates are obtained by multiplying the integral of the column abundance along each transect by the wind speed at the plume altitude (Pugnaghi et al., 2006; Corradini et al., 2009; Merucci et al., 2011; Theys et al., 2013). This method implicitly assumes an infinite lifetime for SO_2 and ash during the emission inversion. This could lead to an underestimation of the emission rates.

We wish to mention that SO_2 columns may also be obtained from high spectral resolution TIR observations, like those from IASI (Infrared Atmospheric Sounding Interferometer) (see, e.g., Clarisse et al., 2012) or TES (Tropospheric Emission Spectrometer) (Clerbaux et al., 2008).In principle, a better spectral resolution potentially leads to smaller retrieval errors. We have retrieved SO_2 columns with IASI for the 26 October 2013 and found a spatial distribution very similar to the MODIS observations for the same day (results not shown in this paper). In any case, for the present study and the detailed analyses proposed in this paper, MODIS observations have been preferred due to a better spatial resolution and coverage, which allow a more direct comparison and synergy with the Lagrangian modelling described in Sect. 2.3.1.

2.2.2 Ash retrieval from MODIS TIR data

The retrieval algorithm (Dubuisson et al., 2014) is based on the split window technique and uses MODIS brightness temperatures at 11 and 12 μm and accurate radiative transfer calculations with a fast radiative transfer code using the discrete ordinate method (FASDOM) (Dubuisson et al., 2005). In this algorithm, pixels are first classified as containing volcanic aerosol using a detection threshold on brightness temperatures. A set of brightness temperatures is then pre-calculated with the FASDOM code, for the channels at 11 and 12 μm, using realistic aerosol properties and the atmospheric profile obtained from atmospheric soundings performed at Trapani. The effective radius r_e used in the calculations varies from 0.5 to 20.0 μm, and the aerosol optical thickness τ_a at 12 μm from 0 to 10. Look-Up tables of single scattering optical properties for several mineral compositions (andesite, ash, basalt, hematite, obsidian, quartz) and sulphate aerosols are used. The optical properties

8

are calculated with Mie theory using the complex refractive indices reported in the HITRAN database (Rothman et al., 2013). Within each considered pixel, τ_a and r_e are obtained from the observed brightness temperatures at 11 and 12 µm through linear interpolation from the set of pre-calculated brightness temperatures. For a given pixel, a solution is sought
5 separately for each particle type; the retrievals are then averaged.

2.2.3 Cloud top pressure observations from SEVIRI

The Spinning Enhanced Visible and Infrared Imager (SEVIRI) onboard MSG (METEOSAT Second Generation) geostationary satellites (http://www.eumetsat.int/website/home/Satellites/index.html) is a visible and infrared multi-channel imager which is oper-
10 ated on a 15 minute repeat cycle. The sub-satellite point spatial resolution is $3 \times 3\,\text{km}^2$, and the pixel dimension in our region of interest (near Lampedusa) is about $4.3 \times 3.3\,\text{km}^2$.

The cloud top pressure used here is obtained from the Satellite Application Facility for NoWCasting (SAFNWC) algorithm developed by Derrien and Le Gléau (2005, 2010) for MSG-SEVIRI. The SAFNWC algorithm requires, as ancillary inputs, surface height
15 maps, land/sea mask, climatological maps of SST (sea surface temperature), continental reflectance maps, and temperature and humidity profiles. Recently, this algorithm was adapted to other geostationary data and verified using CALIOP (Cloud-Aerosol Lidar with Orthogonal Polarization) data (Sèze et al., 2014). The first two steps of the SAFNWC algorithm, cloud detection and classification, rely on multi-spectral threshold tests applied
20 at the pixel scale to a set of spectral and textural features. Thresholds are tuned to the radiometer's spectral windows with respect to simulated signals in cloud free conditions.

Cloudy pixels are separated into two classes: (1) fractional cloud and high-altitude semi-transparent cloud, (2) low, medium, and high thick clouds. Using the same technique, pixels falling in the first class are divided into fractional, high semi-transparent cloud, and high
25 semitransparent in a multi-layered cloud system. The opaque cloud top pressure is retrieved from the 10.8 µm brightness temperature and ancillary temperature and humidity profiles. For low and middle clouds, tests are applied to place the cloud top level below an existing temperature inversion. A correction for semi-transparency is applied to the high thin clouds

9

using two IR channels, a window, and a sounding channel (13.4, 7.3, or 6.2 μm), as in the paper by Schmetz et al. (1993). No pressure information is available for pixels belonging to the partially cloudy class; clouds partly covering these pixels can be at any level in the atmosphere.

2.3 Model simulations

2.3.1 Plume dispersion simulations with FLEXPART

We simulate the dispersion of the sulphur dioxide and ash plumes with the Lagrangian dispersion model FLEXPART (FLEXible PARTicle dispersion model) (Stohl et al., 2005). Both sulphur dioxide and ash simulations are initialised with the emission rates estimated by MODIS using the methods described in Sect. 2.2.1 (synergy (a) identified in Fig. 1). Our FLEXPART simulations use European Centre for Medium-Range Weather Forecasts (ECMWF) meteorological data at $0.1° \times 0.1°$ horizontal resolution and 137 height levels (100–200 m vertical resolution in the troposphere, 1–2 km in the lower stratosphere). The simulations extend over the period of the main eruption activity, concurrent to the availability of the emissions, from 26 October, 05:00 to 26 October, 12:20. The simulations of the SO_2 plume dispersion are extended to 26 October, 21:00 to analyse the further dispersion of the SO_2 plume. The sulphur dioxide emissions are assumed to be constant at a very small degassing background after 12:20; as can be seen from the discussion of the event in Sect. 3, most of the sulphur dioxide emission has finished by that time. The FLEXPART outputs are averaged over 20 minute intervals and are given at 16 altitude levels, from the surface to 14 km altitude, with a vertical resolution ranging from 0.5 to 2.0 km.

The lifetime of the SO_2 is determined by dry and wet deposition and chemical losses for the oxidation to sulphuric acid. It can be roughly estimated from the generic residence time equation (see, e.g., McCormick et al., 2014):

$$\tau = \frac{M}{Q} \tag{1}$$

10

where τ is the lifetime, M is the SO$_2$ mass loading and Q is the SO$_2$ emission rate. From mass loading and emission rates derived from MODIS (see Sect. 2.2.1), we derived an SO$_2$ lifetime of 6.7 h for the image of 26 October 2013, 12:20 (synergy (b) identified in Fig. 1). We then considered a fixed lifetime of 6.7 h (loss rate of about $4.2 \times 10^{-5}\,\mathrm{s^{-1}}$) for the sulphur dioxide in our simulations for that day. It must be noted that using a fixed value for the SO$_2$ lifetime is a simplified approach and more refined estimations (time- and atmospheric parameters-dependent) could be obtained using detailed chemistry modelling, as mentioned in Sect. 2.1. It must also be noted that, as stated in Sect. 2.2.1, the emission rate Q is likely underestimated, with the result that the lifetime τ could be overestimated. Estimates of the SO$_2$ lifetime and loss rate were previously obtained in several measurement campaigns. The observed values of loss rates are variable, and range, worldwide, from about 3×10^{-7} to $10^{-3}\,\mathrm{s^{-1}}$ (Oppenheimer et al., 1998). Values between about 3×10^{-6} to $4 \times 10^{-5}\,\mathrm{s^{-1}}$ are found for Mount Etna (Oppenheimer et al., 1998). Quicker loss rates, up to $10^{-3}\,\mathrm{s^{-1}}$ can occur in cases of high humidity or high ash burden in the plume (McGonigle et al., 2004). The value of the sulphur dioxide loss rate we obtain is consistent with these previous determinations for Mount Etna. An SO$_2$ point injection at 7000 m has been assumed. As pointed out later, SEVIRI cloud top observations fully confirm this assumption (synergy (e) identified in Fig. 1).

Ash simulations take into account both gravitational settling, and (wet and dry) deposition. However, ash aggregation processes are not taken into account. Six ash classes are modelled, based on a typical ash size distribution obtained with the mk_releases.f routine (courtesy of Nina Kristiansen and Andreas Stohl), based on the work of Mastin et al. (2009). The central radii and the percent population of each class in the ash distribution are listed in Table 1. This distribution can be roughly approximated with a bi-modal log-normal size distribution (geometric mean radii of 1.0 and 10.0 µm, geometric standard deviation of 2.3 and 2.0, respectively), representing both fine and coarse ash particles (Dulac , 2015). This size distribution is consistent with that observed in deposited ash and from airborne (see, e.g., Stohl et al., 2011) or remote sensing observations. Sun photometric measurements (see, e.g., Watson and Oppenheimer, 2000) performed at Mount Etna have shown a tri-

11

modal log-normal aerosol size distribution, with a coarser mode with a mean radius greater than 5 µm, which is partially attributed to ash during relatively weak activity phases. Coarse modes with higher mean radii, greater than 10 µm, are observed in eruptive size distributions, (e.g., at Mount Redoubt, AK, USA) and attributed to ash particles (Hobbs et al., 1991).

5   In addition, a campaign has been conducted at the beginning of October 2013, to characterize Etna's emissions with in-situ measurements of different gases and aerosols properties. Bi- and tri-modal aerosol size distributions were observed during this campaign, with the coarser modes identified as ash (T. Roberts, personal communication). These latter modes exhibited log-normal distributions with mean radii and widths similar to the ash size distri-

10 bution used in our simulations. These direct observations at Etna, for a period of only a few days before our study, justify our ash size distribution assumption, even if coarser particles can be observed during an eruption event. Following Mastin et al. (2009), we model the vertical distribution of the emissions using four layers, from the Mount Etna summit (about 3300 m above sea level) to the plume height, 7000 m above sea level for our simulations,

15 with a maximum of the ash injection (60 %) at the plume top altitude and rapidly decreasing injection quantities in the lowest 3 levels (25, 10, 5 % at about 6000, 5000 and 4000 m).

2.3.2 Radiative transfer simulations with LibRadtran/UVSPEC

We investigate the possible radiative impact of the Mount Etna plume for the event under investigation by estimating the shortwave clear sky direct radiative forcing at the surface

20 and at the top of the atmosphere (TOA) with the radiative transfer model UVSPEC and the LibRadtran package (Mayer and Kylling, 2005). The method chosen for the solution of the radiative transfer equation is SDISORT, the pseudo-spherical approximation of the discrete ordinate method (DISORT) (Dahlback and Stamnes, 1991). Surface and TOA spectra are calculated in the shortwave spectral range, from 300.0 to 3000.0 nm, at 0.1 nm spectral

25 resolution. The input solar flux spectra is described in Kurucz (1994). Vertical profiles of temperature, pressure, humidity and gases concentration are derived from the AFGL (Air Force Geophysics Laboratory) climatological standard atmosphere (Anderson et al., 1986). Molecular absorption is parametrised with the LOWTRAN band model (Pierluissi and Peng,

1985), as adopted from the SBDART code (Ricchiazzi et al., 1998). The aerosol optical and micro-physical properties are based on prescribed aerosol models, as described by Shettle (1989). We have selected a moderate volcanic aerosol layer at altitudes higher than $2.0\,\text{km}$, among the available aerosol models. Then the optical characterization of the layers can be refined by means of the extinction coefficient vertical profile, the single scattering albedo, the Ångström parameter and the asymmetry factor. In this case we have corrected the aerosol optical properties by means of the observed single scattering albedo, the observed Ångström exponent, the observed asymmetry parameter (synergy (g) identified in Fig. 1), and the modelled vertical distribution (synergy (f) identified in Fig. 1). A detailed description of the aerosol set-up in the model is given in Sect. 7. The surface albedo (independent from wavelength) is set to 0.09, as done by Meloni et al. (2003)

The UVSPEC model gives as outputs the downward direct and diffuse, and the upward diffuse irradiances. In general, the shortwave aerosol radiative forcing at a fixed altitude is the difference between the net flux (downward minus upward irradiance) with and without aerosols, integrated over the shortwave spectral range. The shortwave TOA radiative forcing ΔF_{TOA} of a given aerosol layer is then defined as the upward diffuse irradiance for a baseline simulation without aerosols minus that with aerosols, integrated over the whole spectral range. The shortwave surface radiative forcing ΔF_{surf} is defined as the downward global (direct plus diffuse) irradiance with aerosols minus baseline, integrated over the whole spectral range.

2.4 Surface remote sensing observations at Lampedusa

Many parameters related to climate are routinely measured at the ENEA Station for Climate Observations on the small island of Lampedusa (35.5° N, 12.6° E), in the central Mediterranean. The measured parameters include greenhouse gases (Artuso et al., 2009), aerosol optical and chemical properties (Di Iorio et al., 2009; Marconi et al., 2014), total ozone, spectral and broadband irradiances (Meloni et al., 2005a; Di Biagio et al., 2010; di Sarra et al., 2011).

13

A Brewer double monochromator (Kerr et al., 1985), model MK III, is operational at Lampedusa since late 1997. Column sulphur dioxide measurements used in this study are derived from direct sun solar radiation measurements at several UV wavelengths; sulphur dioxide column is retrieved jointly with total ozone (e.g. Georgoulias et al., 2009).

Measurements of aerosol optical depth and Ångström exponent at several wavelengths are carried out with a Cimel sun-photometer, and in parallel with a Multi Filter Rotating Shadowband Radiometer (MFRSR) (e.g. di Sarra et al., 2011, 2015). The Cimel sun-photometer is part of the AErosol RObotic NETwork (AERONET, see the AERONET website http://aeronet.gsfc.nasa.gov and the description by Holben et al. (1998) for further details). The total aerosol optical depth is separated into the fine mode and coarse mode components by means of the Spectral Deconvolution Algorithm (SDA), developed by O'Neill et al. (2003). In addition, size distributions are derived from almucantar observations (Dubovik and King, 2000).

3   The eruption of Mount Etna of 25–27 October 2013

The eruption explored in this study occurred between 25 and 27 October 2013. The plumes of emitted ash and gases were observable for a few more days. This eruption was the 14th episode occurring in 2013, and the 39th of the eruptive sequence started in January 2011 (Calvari et al., 2011; Patanè et al., 2013). Figure 2 shows the episode (from the point of view of the plumes) by means of a composition of four Aqua- and Terra-MODIS true colour images (available at the website: http://modis-atmos.gsfc.nasa.gov). These true color images give a general view of the plume, which is directly observable in the visible channels (thick ash plumes, clouds). A more complete characterization of the atmosphere is obtained using MODIS thermal infrared channels and spectroscopic methods (see, e.g., Sects. 4 and 5). The eruption began at the New South East Crater (NSEC) on 25 October, at about 12:45, feeding strombolian activity initially confined to the crater. The MODIS satellite images show a very localised plume from Mount Etna on 25 October (Fig. 2a), maybe linked to this early discontinuous volcanic activity. Almost 4 hours later, the number, intensity, and frequency of

explosions steadily intensified evolving transitionally to a lava fountain on 26 October, about 02:00. Rapidly, a dense and sustained-thick ash plume formed, initially identified at about 7 km altitude. Most of the fallout spread south-westward across the Mediterranean Sea (INGV, 2013a). At about 06:20 the eruption of a secondary ash-rich cloud started from the
5 North East Crater (NEC), coupled with irregular explosive activity at Bocca Nuova crater. The emitted material reached 7 km altitude. After about 10:00 the lava fountaining intensity decreased substantially, switched to strombolian activity and gradually ended at about 13:00. A thick plume is visible in the MODIS images of 26 October (Fig. 2b–c) from Mount Etna towards the south-west. Ash emission from NEC became progressively moderate and
10 intermittent, persisting until about 00:00 of 27 October, when the activity eventually stopped, as evident from Fig. 2d and later MODIS imagery. Three lava flows were emplaced on the south-east summit area of Mount Etna, remaining active until late afternoon of 26 October. The eruptive episodes produced abundant ash emissions, whose fallout dispersed hundreds of km south of the volcano (INGV, 2013b). Figure 3 shows bi-hourly forward trajecto-
15 ries of the volcanic plume (Fig. 3a), i.e., the projection of the centroid of the sulphur dioxide plume on the horizontal plane, and the time evolution of its average altitude (Fig. 3b), i.e., of the projection of the centroid of the sulphur dioxide plume on the vertical axis, for the whole period under investigation, as obtained from the FLEXPART simulations. Airmasses from Mount Etna overpassed Lampedusa during 26 October 2013 (in red) and 27 October 2013
20 (in violet). While the plume had, on average, descending trajectories from the assumed injection altitude (7 km) to lower altitudes, individual trajectories on 26 October 2013 showed events of lofted airmasses, e.g., a few hours after the trajectory initialisation. This feature and its implications are thoroughly discussed in Sects. 4, 5 and 6.3.

The method described in Sect. 2.2.1 was applied to the Aqua-MODIS observations of
25 26 October, at 12:20, to estimate the rate of sulphur dioxide and ash emissions during the most intense phase of the eruptive event. We considered a wind speed of $18\,\mathrm{m\,s^{-1}}$, constant with time and altitude. This value is representative of the mean wind speed between 410 and 165 hPa, approximately 7 and 13 km altitude ($18.0 \pm 5.9\,\mathrm{m\,s^{-1}}$, based on the radiosounding of 26/10/2013 12:00 UTC at Trapani WMO station). Nevertheless, the variability

15

with altitude and time is relatively important and then more refined approaches, based on variable wind speed values, can be envisaged in the future. This inverse method allows the reconstruction of the emissions during the eruptive event, going several hours backwards in time. The temporal evolution of the emissions is shown in Fig. 4.

The SO_2 and ash emissions started in the early morning of 26 October, and sharply increased from 08:00 to 12:00. Emission estimates for 26 October reached 1700 and 800 $kg s^{-1}$, for SO_2 and ash, respectively. This temporal evolution was consistent with the qualitative description of the event given by INGV (Istituto Nazionale di Geofisica e Vulcanologia) (INGV, 2013a). The SO_2 emissions rates are routinely measured at Mt. Etna by INGV since the year 2000, using ground-based ultraviolet spectroscopy techniques (e.g., Salerno et al., 2009a). It is well known that matching between ground- and satellite-based SO_2 emissions estimations might display large discrepancies, due to plume height uncertainties, and sulphate aerosol, ash and ice in the volcanic plume, that may introduce over- or under-estimation of the SO_2 burden in both ground- and satellite-based retrievals (Boichu et al., 2015, and references therein). A direct comparison of the estimates from the two methods is beyond the scope of this study; instead we employ the ground-based SO_2 emissions for classifying the magnitude of the 26 October episode. This allows a self-consistent classification of the atmospheric-impact strength of this event with respect to the eruptive style and activity, on a more-than-decennial time-scale. The mean value of the SO_2 emissions rate in the time interval 2001–2011 is about 2500 $t d^{-1}$ (tons per day) (Salerno et al., 2009b; Giammanco et al., 2013; Patanè et al., 2013), with about 1850 $t d^{-1}$ for the passive-degassing-only activity and with the highest emission rates reaching about 30 000 $t d^{-1}$ during major Etna's eruptive crises (INGV, 2013b). Thus, the emission rate measured on 26 October, of about 1200 $t d^{-1}$, suggests that the 26–27 October event was a relatively weak eruption with respect to the SO_2 emissions (synergy (c) identified in Fig. 1). It should be noted that the ground-based spectroscopic emissions measurements were not available for a few hours during the main phase of the eruption and, correspondingly, the retrieved emissions rate was likely underestimated.

16

4 Dispersion of the sulphur dioxide plume: satellite observations and Lagrangian analysis

As mentioned in Sect. 3, 26 October is characterised by the strongest activity during the case study. We therefore study in more detail the emissions occurring during this day and the dispersion of the plume.

Figure 5a shows the sulphur dioxide column abundance in the Central-South Mediterranean, as obtained from the Aqua-MODIS image of 26 October 2013, 12:20. The inversion algorithm described in Sect. 2.2.1 is used, with a volcanic cloud top altitude of 7 km. The SO_2 plume from Etna, heading south-west, is evident.

The column abundance reaches values as high as $4.5\,t\,km^{-2}$, in the region South of the island of Pantelleria. The plume passes about 100 km North-West of Lampedusa.

Satellite SO_2 observations can provide only a partial information on the sulphur dioxide height distribution, e.g., the injection altitude with an assumed vertical distribution (Carboni et al., 2012). The vertical distribution of sulphur dioxide may give important indications on the potential impact of these emissions on the aerosol composition in the area, through the formation of secondary sulphate aerosols with different lifetimes, which, in their turn, depend on altitude. The lifetime of sulphate aerosols at $35°\,N$ is considerably longer in the upper than in the lower troposphere, e.g., 1–2 months at 10 km and a few days at 5 km altitude, (see Fig. 3 in Stevenson et al., 2003). Thus, the sulphate burden is more strongly affected by sulphur dioxide injected at high altitude (Graf et al., 1997). We coupled the available satellite observations with modelling of the plume dispersion to derive a more detailed description of the SO_2 evolution (synergy (d) identified in Fig. 1). We performed a height-resolved analysis of the plume dispersion with the FLEXPART model (please refer to Sect. 2.3.1 for more details). The FLEXPART simulations were initialised with the sulphur dioxide emissions of Fig. 4, and take as input the SO_2 lifetime estimated from MODIS observations. Figure 5b shows the sulphur dioxide total column abundance from FLEXPART simulations for 26 October, 12:20.

Both the modelled and observed sulphur dioxide plumes are oriented towards southwest, and are characterised by a mean column amount between 2 and 3 t km^{-2}. While the far-range downwind SO_2 distributions in the plume are quite consistent, some differences in the peak position are present in the region close to the source. These differences suggest
5 that the SO_2 lifetime is longer, the time-evolution of the emissions is different, or the winds are stronger than those used in our simulation. The MODIS-derived SO_2 abundances might also be underestimated near-source because of the presence of cirrus clouds, as shown in Fig. 8. Starting from the overall consistency of modelled and observed SO_2 plume, we try to get more insights into its vertical distribution, using the FLEXPART simulations.

10 Figure 6a shows the sulphur dioxide vertical profile along section *T* in Figs. 5b and 6b. Figure 6b shows the spatial distribution of the sulphur dioxide volume mixing ratio (VMR) in the altitude range 10–14 km.

The vertical distribution shows the presence of sulphur dioxide in the upper troposphere within the region located about 200 to 400 km downwind of Etna along *T*. By inspecting the
15 spatial distribution of sulphur dioxide mixing ratio at 10–14 km, values of up to 60 ppt (part per trillion) are found a few tens of km from Lampedusa, and up to 300 ppt less than 100 km northwards. Values greater than about 100 ppt are considered a significant perturbation from background values, and are expected to perturb the secondary sulphate aerosol content (Doeringer et al., 2012).

20 The spatio-temporal evolution of the SO_2 VMR in the altitude range 10–14 km is reported in Fig. 7. Maps are displayed every hour, from 09:20 to 20:20. The upper tropospheric plume appears at 10:20 and develops in the following hours moving mostly southwards. It stays in the area of Lampedusa for several hours, partly overpassing the island between 15:20 and 18:20. This is consistent with the presence of relatively long-lived sulphate aerosols over
25 Lampedusa, starting from 26 October in the late morning and early afternoon.

To further investigate the injection altitude of the volcanic plume, we use the SEVIRI cloud top pressure product described in Sect. 2.2.3 (synergy (e) identified in Fig. 1). These observations permit the reconstruction of the airmass altitude evolution at high temporal resolution. The altitude of the sulphur dioxide injection and vertical motions in the proximity

18

of the volcanic source play a role in the lifetime of the sulphate aerosols produced, in the duration of the perturbation, and in the impact on the aerosol properties at the regional scale. Figure 8 shows cloud top pressure images for selected time intervals, providing a description of the different phases of the eruption. Figure 8a–c shows the initial phases of the event. The discontinuous emissions in the first phase occurred with injection at low altitudes (cloud top altitude at 3.5 km, close to the Mount Etna summit), as appears at 05:30 (Fig. 8a); the plume developed starting from 06:00, and reached the initial injection altitude of 7.0 km in the next few tens of minutes (Fig. 8b–c); the plume then headed towards the South-West, following the prevailing winds. It is worth noting that these results confirm the assumption of 7.0 km altitude as the plume top height. This value is used to initialize both the inversion algorithms for MODIS, and the FLEXPART simulations. The SEVIRI observations show two successive events of lofted airmasses on the plume trajectory, the first in the time interval 07:00–07:30 (Fig. 8d–f), and the second in the time interval 08:45–09:15 (Fig. 8g–i). Both events are characterised by cloud tops reaching altitudes of about 11.0 km, with the lifting occurring some tens of km downwind of the Etna summit. This evidence is consistent with the sulphur dioxide vertical concentration profile along T shown in Fig. 6a, where a region of lofted airmasses can be observed at grid-points 0–150, in approximately the first 100 km along T (from Mount Etna to southern Sicily). Thus, the SEVIRI observations fully justify the presence of sulphur dioxide emitted from Mount Etna at altitudes higher than the initial injection.

5 Dispersion of the ash plume: satellite observations and Lagrangian analysis

Similarly to the sulphur dioxide plume, we characterize the ash plume and its dispersion by means of MODIS observations and FLEXPART calculations (synergy (d) identified in Fig. 1). Figure 9a shows the spatial distributions of optical depth at 550 nm, obtained using the inversion algorithm described in Sect. 2.2.2.

The mineralogical composition of the ash plume is primarily andesite, basalt, hematite and quartz. The mean plume optical depth is 0.34. The spatial distribution of the optical

depth is consistent with the sulphur dioxide plume described in Sect. 4. The ash plume has a similar downwind orientation towards the South-West. The optical depth has values higher than 1.5 near the source and decreases rapidly to values smaller than 0.2 downwind. Satellite ash observations in the TIR are only sensitive to coarse particles (Stephens, 1994;

5 Stohl et al., 2011). A relatively detailed size-resolved modelling of the ash plume, especially for the fine ash component, is however crucial to assess the impact of moderate volcanic eruptions on downwind aerosol micro-physical and optical characterization. This would allow disentangling the impact of the sub-micron sized sulphate aerosols, possibly formed from the sulphur dioxide gas-to-particle conversion, from that of the fine ash component.

10 The FLEXPART model is initialised with the ash emissions shown in Fig. 4 and with the size distribution of Table 1. We recall that we consider a typical size and vertical distribution and simulate 6 aerosols classes, as a function of size (see Table 1). The use of a given size distribution allows us to separately investigate the dispersion for the different size classes. The modelled total ash column abundance is shown in Fig. 9b. We sum the concentrations

15 of classes 3, 4, and 5, at which TIR measurements are more sensitive, (e.g., Fig. 1 of Stohl et al., 2011), to compare with the MODIS observations. The shape and the relative amounts along T are consistent with the MODIS observations of Fig. 9a, with column abundances peaking at the source and decreasing along T.

The vertical distribution along T is shown in Fig. 10 for the 6 size classes. The same

20 lifting structures observed in the simulations of the SO_2 plume and identified by the SEVIRI cloud observations are observed for the ash plume dispersion. The behavior of fine ash can be associated with the evolution of class 1 particles (central radius of 0.2 μm). The fine ash seems not capable of reaching the area of Lampedusa (gridpoint 340–350 along T, a few tens of km North of Lampedusa). Also for the other classes, the impact of the

25 ash particles seems more local, with steep negative gradients of the ash concentrations along T for all the 6 classes. The smaller ash emission rates for this event (compared to the SO_2 emission rates), and the very limited contribution of the finer particles (1 % for the class 1 – central radius at 0.2 μm, see Table 1) for a typical ash distribution at Mount Etna are responsible for the relatively small-range impact of finer ash particles. Here we want

to stress that the fine ash is not directly observable by TIR measurements, due to their weak sensitivity to small particles. Thus, the combined approach based on the synergy of modelling and observations may allow a better insight of the phenomenon than modelling or observations alone.

6   Plume downwind signature at Lampedusa and discussion

The effects of the volcanic emissions downwind Mount Etna can be observed at the central-Southern Mediterranean station of Lampedusa. This station is well suited for the analysis of this specific event, due to the prevailing meteorology during the period 25–27 October 2013. As shown in Fig. 2e, airmasses from Mount Etna overpass Lampedusa during 26 and 27 October 2013, and it is reasonable to search for a signature of this eruptive event on the sulphur dioxide and aerosol measurements at Lampedusa. It is worth mentioning that Lampedusa is one of the supersites involved in the ChArMEx experiment (Mallet et al., 2016).

6.1   SO$_2$ observations

We first investigate the Brewer SO$_2$ measurements. Thanks to the frequent cloud-free conditions occurring in late October, many valid direct Sun measurements (more than 30 per day) were obtained during the event. The total sulphur dioxide displays a limited variability during the period (not shown here), with moderately low amounts (generally below 2.5 DU – Dobson Units). No strong increase is observed in the days of the eruption. However, when calculating the 5-day running mean of the daily total sulphur dioxide measurements, a small enhancement is found (5-day average of about $+2.0$ DU throughout the period 27–31 October). These observations suggest a limited direct impact at Lampedusa of the sulphur dioxide emissions from Etna. While our FLEXPART simulations show the presence of sulphur dioxide in the Lampedusa area, particularly at higher altitudes, their concentrations might be under the detection limit of the Brewer total SO$_2$ column observations. It is worth mentioning that the SO$_2$ plume following this eruption and a small but clear en-

hancement (up to 1.5–2.0 DU) of the SO_2 column with respect to background values are observed in the area of Lampedusa by the Ozone Monitoring Instrument (OMI), OMSO2 Level 2 product, for 27 October 2013 (Krotkov et al., 2006) (data publicly available at: http://so2.gsfc.nasa.gov/pix/daily/ixxxza/loopall3.php?yr=13&mo=10&dy=27&bn=etna). An

5   isolated maximum is also observed in the SO_2 mass burden daily time-series for October 2013, in the Etna region for this day (data publicly available at: http://so2.gsfc.nasa.gov/pix/daily/1013/etna_so2lf_5k_ts_plot.html). OMI data are not available for 26 October 2013 due to an interruption of operations.

6.2   Aerosol optical and micro-physical properties

10   Aerosol optical depth, its fine and coarse component and Ångström exponent (derived using pairs of simultaneous aerosol optical depth observations at 440 and 870 nm) measurements are shown in Fig. 11a–b. Measurements show relatively low values of the total aerosol optical depth (less than 0.2) throughout the event. At the same time, a steep variation of the fine-to-coarse optical depth fraction is observed from 26 October. The average fine-to-

15   coarse aerosol optical depth fraction is $77.6\% \pm 3.5\%$ for the period 26–29 October, while it is $49.0\% \pm 18.2\%$ for the whole month of October 2013. In addition, elevated values of the Ångström exponent, i.e., between 1.5 and 1.7, are observed in the period 26–29 October. The average Ångström exponent is 1.61 ± 0.06 in the period 26–29 October, while it is 0.92 ± 0.44 for the whole month of October 2013. The Ångström exponent values observed

20   on 26–29 October are very high for Lampedusa (see, e.g., Meloni et al., 2007), especially in the early fall season. In the dataset of aerosol optical properties at Lampedusa, covering the period 2001 to present, there is no other case with similar values of the Ångström exponent and fine-to-coarse aerosol optical depth fraction in late October. This case stands out as an anomaly in the Lampedusa record, and suggests an unusually large population of fine

25   particles.

A further indication of the aerosol size distribution changes occurring at Lampedusa is shown in Fig. 12, where average volume size distributions are shown before, during, and after the eruption event. The coarse mode, which is predominant in the period 1–24 October

22

and is still evident on 25 October, falls quickly on 26 October, while the fine mode becomes more important (more than two times larger than in the pre-eruption period), with increasing mode radius (from a pre-eruption value of about 0.1 to about 0.2 μm). The size distribution changes in the following days, to return to pre-eruption conditions after 29 October. All these

5 observations seem to indicate a signature of the Etna's plume over Lampedusa from 26 to 29 October, suggesting the presence of small particles of volcanic origin. The lack of clear indication of very small aerosols after the 29 October at Lampedusa seems to be related to the displacement of the airmasses affected by the eruption following the prevailing winds.

6.3 Role of sulphate aerosols and ash at Lampedusa

10 The signature of the Etna plume observed at Lampedusa can be attributed to volcanic fine ash particles and secondary sulphate aerosols formed by the conversion of the SO_2 gaseous emissions. It is worth mentioning that, while in this discussion we assume that all the sulphate aerosols are produced as secondary particles, a relatively small amount of primary sulphate particles can be emitted by volcanoes like Mount Etna, as shown by

15 near-source observations (e.g., Martin et al., 2008).

Higher values of the Ångström exponent, e.g., greater than 1.0, are associated with non-ash-bearing volcanic plumes (e.g., Watson and Oppenheimer, 2000; Mather et al., 2004). In particular, the Ångström exponent values observed at Lampedusa (average value of 1.61 ± 0.06 for the period 26–29 October) are consistent with those measured in the Mount

20 Etna near source plume in the past. Watson and Oppenheimer (2000) and Watson and Oppenheimer (2001), for example, measured a number of optical parameters of Mount Etna aerosol plumes by sun-photometry and found a mean value of the Ångström exponent of 1.67, during a non-eruptive short time period in October 1997, and of 1.63 for a non-ash-bearing plume during July 1999.

25 The nucleation and accumulation modes in the tri-modal number size distributions measured in the past at Mount Etna by sun-photometry display maxima at about 0.1–0.2 and at 0.6–0.9 μm, respectively, with up to three orders of magnitude difference between the nucleation and the accumulation mode (Fig. 6a of Watson and Oppenheimer, 2000, Fig. 4a

of Watson and Oppenheimer, 2001), thus generating a size distribution characterised by markedly increasing concentrations for very small radii. Similar size distributions are observed at Lascar and Villarrica volcanoes, Chile (Mather et al., 2004). Thus, the nucleation mode seems to dominate non-ash volcanic plumes, and the transport of the nucleation

5 mode aerosols (mean radius less than 0.1–0.2 µm) or the nucleation of new particles downwind might explain the large contribution to the fine mode aerosols at Lampedusa, as shown in Fig. 12.

Single scattering albedo (SSA) retrievals could give an indication of the presence of weakly absorbing sulphate particles. The average observed value of the single scattering

10 albedo in the visible (about 440 nm) is 0.93 ± 0.04 for the period 26–29 October, with the highest daily value of 0.98 ± 0.01 for 26 October. The average SSA for the whole month of October 2013 is 0.91 ± 0.05. This might indicate the presence in the period 26–29 October of particles with the typical optical properties of the very weakly absorbing sulphates. However, it must be noted these retrievals have significant uncertainties, as expected for cases

15 with relatively small aerosol optical depths (less than 0.2).

The unequivocal attribution to one of the two sources (fine ash or secondary sulphate aerosols) is impossible at this stage due to the lack of specific measurements of the chemical composition of the aerosols, or a simulation of the sulphate aerosols chemical/microphysical evolution, as mentioned in Sect. 2.1. Instead, we exploit our synergistic approach

20 to infer the prevailing composition of the volcanic aerosol at Lampedusa. Due to the considerations in Sect. 5 (the size-dependent ash dispersion analysis indicates a limited fine ash component at Lampedusa), we speculate that fine ash particles had a very small impact on the measurements at Lampedusa (synergy (h) identified in Fig. 1). Conversely, the discussion in Sect. 4 (the height-resolved SO_2 dispersion analysis indicates that SO_2 con-

25 centrations are significantly higher than background levels in the upper troposphere over Lampedusa), the comparison of micro-physical aerosol properties at Lampedusa with data in the literature, and the indications of favourable conditions for the formation of new particles through gas-to-particle conversion, suggest that the secondary sulphate particles may

24

be the primary cause for the observed aerosol optical properties and their evolution following the eruption.

7 Estimates of radiative effect

Radiative transfer simulations were carried out with the LibRadtran/UVSPEC model, as described in Sect. 2.3.2, to obtain a rough estimate of the clear sky direct radiative effects produced by the aerosols in the volcanic plume for this event. The aerosol input parameters are based on the observations at Lampedusa described in Sects. 6.2 and 6.3 (synergy (g) identified in Fig. 1). The Ångström exponent is set at the mean value observed in the period 26–29 October (1.61). We have considered different values of SSA, given the daily variability of this parameter and the measurement uncertainties. This allows us to estimate the sensitivity of the radiative forcing to aerosol absorption. We have run the model using SSA values of 0.93 (mean value for the period 26–29 October), 0.97, 0.98 and 0.99 (mean daily value for 26 October minus and plus one standard deviation). The asymmetry parameter was set to the value of 0.70, following AERONET observations at Lampedusa for 26 October. Since it is not possible to quantify the contributions to the total AOD from lower tropospheric aerosols and from volcanic particles, we have used a single aerosol type with the measured AOD, Ångström exponent, SSA and asymmetry parameter in the model setup. Thus, the simulated radiative forcing is relative to the whole aerosol column. It must be noticed however, that we expect to have marine particles in the lower troposphere, but the observed integrated Ångström exponent is much higher than expected for sea salt aerosols. The stratospheric aerosol optical depth is considered negligible during this event. In fact, while the stratospheric aerosol layer has enhanced particle concentration and optical depth in the period 2000-2010, due to the occurrence of a series of moderate stratospheric volcanic eruptions, this layer has returned to background values by 2013 (a stratospheric aerosol optical depth of about 0.005-0.008, see Fig. 1a of Ridley et al. (2014)). Thus, we assume that the upper tropospheric volcanic particles produced during this eruptive event are dominant in the column on 26 October. Following the indication given by the

25

FLEXPART plume simulations, e.g., the SO_2 plume vertical profile of Fig. 6a, we consider a volcanic aerosol layer between 8 and 14 km (synergy (f) identified in Fig. 1). We have tested different vertical profiles of the AOD in this interval but found that the radiative forcing estimations differ by less than 5%. The weak dependence of the radiative forcing to the aerosol vertical profile has been observed in the past, e.g., by Meloni et al. (2005b). The calculations are made over the 300–3000 nm spectral range, and are integrated to obtain shortwave irradiances at the surface and at TOA. The radiative forcing is calculated for fixed aerosol properties between 0 and 90° solar zenith angle, with 15° steps. The radiative forcing is normalised per unit of AOD, i.e., expressed in radiative forcing efficiency (RFE). The RFE is integrated over 24 hours to obtain the daily RFE.

The estimated daily shortwave RFEs are reported in Table 2 together with the ratio f between the surface and TOA RFEs. Increasingly negative values (-39 to -48 W m^{-2} AOD^{-1}) and decreasingly negative values (-66 to -49 W m^{-2} AOD^{-1}), with increasing SSA, are found. Correspondingly, the ratio f varies between 1.7 (SSA = 0.92) and 1.0 (SSA = 0.99). The radiative forcing is, thus, strongly dependent on the SSA. This evidence has been recently confirmed in a more general context (wider variability of the optical parameters) by Sellitto and Briole (2015). In this latter paper, it has been shown that the RFE is more dependent on the SSA than on the other aerosol optical input parameters used in the present study (the asymmetry parameter and the Ångström exponent), especially when sulphate aerosols are dominant (bigger values of the Ångström exponent and the SSA). As the SSA is the dominant factor in the RFE variability, the formation and evolution processes of volcanic sulphate aerosols is very critical for the downwind radiative impacts and a more detailed description of these processes, i.e., with a chemistry/micro-physics model, would be needed to study this kind of impact, as mentioned in Sect. 2.1.

The estimates of RFE are within the range of previous studies in the Mediterranean (e.g., di Sarra et al., 2008; Di Biagio et al., 2010; García et al., 2012). However, the RFE values depend on the day of the year and on surface albedo, and a direct comparison is not possible. Conversely, the ratio f is less dependent on the day of the year. The value of f decreases for increasing SSA, and is close to 1.1 for the observed daily SSA for

26

26 October. The values of f previously found in the Mediterranean (see, e.g., Table 5 of Di Biagio et al., 2010) are generally higher than those found in this study. Di Biagio et al. (2010) found a value of 1.5, 2.6 and 3.1, with aerosol types identified as desert dust, mixed aerosol and urban/industrial biomass burning particles, respectively. Since, in general, f

5 increases with the aerosol absorption, the volcanic aerosols reaching Lampedusa appear to be less absorbing than other types generally found in the central Mediterranean. In this context, the estimated daily RFEs can be compared with other volcanic sources, like the well documented eruption of Eyjafjallajökull in 2010. The aerosols in the Eyjafjallajökull plume were rich in ash and displayed different optical properties with respect to the Etna

10 plume investigated in the present study. Derimian et al. (2012) estimated the daily TOA and surface RFEs at Lille, France, due to the overpass of the Eyjafjallajökull plume and found values of -31 and $-93\,\mathrm{W\,m^{-2}\,AOD^{-1}}$ ($f = 3$). The large differences between the values of f for the Mount Etna plume under investigation and the Eyjafjallajökull plume support the hypothesis of the major role of sulphates in our case study.

15 The previous discussion applies to RFEs calculated with a wavelength-independent surface albedo value of 0.09. This value has been previously used in radiative forcing calculations at Lampedusa and is considered representative of this particular location (Meloni et al., 2003). Nevertheless, the radiative forcing is strongly dependent on surface albedo (Zhuang et al., 2014). To test the sensitivity to this parameter, we have run further LibRad-

20 tran/UVSPEC simulations with typical: a) sea surface (0.07), and b) desert surface (0.36) albedo values (Briegleb and Ramanathan, 1982). This is intended to test extreme surface characteristics in terms of the albedo. The optical parameters of the volcanic aerosols have been fixed to 1.61, 0.98 and 0.70 for the Ångström exponent, the single scattering albedo and the asymmetry parameter, respectively. The estimated daily shortwave RFEs and fs

25 for the different surface albedo values are reported in Table 3. The estimates for the surface albedo of Lampedusa (0.09) are also shown in the table to more be readily compared with these analyses. The TOA and surface RFEs, as well as the ratio f, vary strongly with the surface albedo. While for typical sea surface albedos the radiative forcing is very similar to the case of Lampedusa's albedo (TOA daily RFE and Surface daily RFE of about -46

and -51 W m^{-2} AOD^{-1} and, correspondingly, f of about 1.0), the radiative forcing varies significantly for typical desert surface albedos (TOA daily RFE and Surface daily RFE of about -14 and -27 W m^{-2} AOD^{-1} and, correspondingly, f of about 1.9). This indicates a significantly smaller negative radiative forcing, for fixed aerosol optical properties. Never-
5 theless, these analyses indicate that the radiative forcing calculated at Lampedusa is likely representative of a large sea surface proportion of the overall Mediterranean region. It must be noted that the use of observed wavelength-dependent surface albedos, like those made by MODIS, would be important towards refining radiative forcing calculations, which is an ongoing work.

10 **8 Conclusions**

Moderate volcanic eruptions may perturb the tropospheric aerosol distribution at different spatio-temporal scales by the injection of both ash and gaseous precursors of sub-micron sulphate aerosols. In this paper we have presented the regional analysis of a minor erup-tion of Mount Etna in late October 2013 by the synergistic use of plume observations and
15 modelling. In our case, this synergy has allowed a better characterization of the plume evo-lution by giving access to useful information which cannot be obtained by observation or modelling alone. Using this synergy, the vertical distribution of SO_2 and ash plumes, the size-resolved ash plume dispersion, and a high temporal resolution of the dispersion may be inferred. The downwind impact on micro-physical and optical aerosol properties are ob-
20 tained using surface remote sensing observations at the well-equipped Lampedusa ground station. It is worth underlining that exploiting a full array of different information sources is of particular importance for moderate eruptions, due to the smaller amount of effluent burden and the inherent smaller sensitivity of the satellite observations. Using this approach, we find that even a minor volcanic event, like the Mount Etna eruption of 25–27 October 2013
25 (SO_2 emission peak of 1700 t d^{-1}, about 20 times weaker than the stronger activity of the years 2000–2003) can significantly perturb the size distribution and the optical properties of the aerosols at the regional scale, with plume signatures detected at a distance greater than

28

350 km from the source. The rapid variation of micro-physical and optical aerosol properties at Lampedusa indicates a strong impact of finer particles. Based on simulations and observations, we are more inclined to attribute this downwind evolution of the aerosol properties to long-lived secondary sulphate aerosol in the upper troposphere than fine ash.

Here we want to mention that an analysis based on SO_2 and ash transport modelling and satellite observations, and aerosol optical properties from ground observations, is necessary because of the lack of reliable sulphate aerosol satellite products and chemistry/microphysics modelling. Dedicated satellite products could allow a direct observation of sulphate aerosols production, life cycle and burden at the regional scale, and chemistry/microphysics modelling could allow the simulation of their formations and evolution processes. Ongoing studies will provide such kinds of satellite products (see, e.g., Clarisse et al., 2013; Sellitto and Legras, 2016) and modelling tools (the coupling of FLEXPART trajectories with sulphate aerosols box models) to simulate these processes are under development.

The sulphate aerosols eventually formed in the plume have the capability to affect the atmospheric radiative transfer through scattering of solar radiation, with a possible influence on the tropospheric photochemistry, and composition. The effects on the radiative balance may be particularly important in the Mediterranean basin, where photochemical processes play a crucial role in the tropospheric chemistry. Daily clear sky direct radiative forcing efficiency (RFE) values are found in ranges between -38.9 and $-47.7\,\mathrm{W\,m^{-2}\,AOD^{-1}}$, at TOA, and between -65.7 and $-48.6\,\mathrm{W\,m^{-2}\,AOD^{-1}}$, at the surface. These values suggest that non-absorbing particles are playing a large role in the local aerosol population, and the absorption by the Etna plume is significantly lower than by desert dust in the central Mediterranean, or by the Eyjafjallayökull plume. The REFs are very sensitive to the surface albedo and to the location where these estimates are performed. Nevertheless, even if these estimates are specific for Lampedusa, the assumed surface albedo is very close to a pure marine albedo and therefore these estimates are representative in a larger area of sea in the Mediterranean.

Studies are ongoing to evaluate the frequency of this type of event, i.e., the transport of volcanically-perturbed airmasses towards the area of Lampedusa. Preliminary results

show that the area of Lampedusa (south-west direction from Mount Etna) is ventilated by airmasses coming from Mount Etna for only about the 5% of the time, in the period 2000-2013 (Sellitto et al., 2016). Correspondingly, the impact of volcanic aerosols (from passive degassing or moderate to explosive eruption) in the central-southern Mediterranean is only episodic. A stronger long-term impact is expected at the same distance in the eastern direction (ventilated for about 80% of the time in the same period, considering south-east to north-east quadrants).

References

Allard, P., Carbonnelle, J., Dajlevic, D., Bronec, J. L., Morel, P., Robe, M. C., Maurenas, J. M., Faivre-Pierret, R., Martin, D., Sabroux, J. C., and Zettwoog, P.: Eruptive and diffuse emissions of CO2 from Mount Etna, Nature, 351, 387–391, doi:10.1038/351387a0, 1991.

Anderson, G. P., Clough, S. A., Kneizys, F. X., Chetwynd, J. H., and Shettle, E. P.: AFGL atmospheric constituent profiles (0–120 km), 1986.

Andreae, M. O.: The Aerosol Nucleation Puzzle, Science, 339, 911–912, doi:10.1126/science.1233798, 2013.

Artuso, F., Chamard, P., Piacentino, S., Sferlazzo, D., Silvestri, L. D., di Sarra, A., Meloni, D., and Monteleone, F.: Influence of transport and trends in atmospheric CO2 at Lampedusa, Atmos. Environ., 43, 3044–3051, doi:10.1016/j.atmosenv.2009.03.027, 2009.

Boichu, M., Clarisse, L., Péré, J.-C., Herbin, H., Goloub, P., Thieuleux, F., Ducos, F., Clerbaux, C., and Tanré, D.: Temporal variations of flux and altitude of sulfur dioxide emissions during volcanic eruptions: implications for long-range dispersal of volcanic clouds, Atmos. Chem. Phys., 15, 8381–8400, doi:10.5194/acp-15-8381-2015, 2015.

Briegleb, B. and Ramanathan, V.: Spectral and diurnal variations in clear sky planetary albedo, Journal of Applied Meteorology, 21, 1160–1171, 1982.

Calvari, S., Salerno, G. G., Spampinato, L., Gouhier, M., La Spina, A., Pecora, E., Harris, A. J. L., Labazuy, P., Biale, E., and Boschi, E.: An unloading foam model to constrain Etna's 11–13 January 2011 lava fountaining episode, J. Geophys. Res.-Solid Earth, 116, B11207, doi:10.1029/2011JB008407, 2011.

Carboni, E., Grainger, R., Walker, J., Dudhia, A., and Siddans, R.: A new scheme for sulphur dioxide retrieval from IASI measurements: application to the Eyjafjallajökull eruption of April and May 2010, Atmos. Chem. Phys., 12, 11417–11434, doi:10.5194/acp-12-11417-2012, 2012.

Carboni, E., Grainger, R. G., Mather, T. A., Pyle, D. M., Thomas, G. E., Siddans, R., Smith, A. J. A., Dudhia, A., Koukouli, M. E., and Balis, D.: The vertical distribution of volcanic SO2 plumes measured by IASI, Atmos. Chem. Phys., 16, 4343–4367, doi:10.5194/acp-16-4343-2016, 2016.

Clarisse, L., Hurtmans, D., Clerbaux, C., Hadji-Lazaro, J., Ngadi, Y., and Coheur, P.-F.: Retrieval of sulphur dioxide from the infrared atmospheric sounding interferometer (IASI), Atmos. Meas. Tech., 5, 581–594, doi:10.5194/amt-5-581-2012, 2012.

Clarisse, L., Coheur, P.-F., Prata, F., Hadji-Lazaro, J., Hurtmans, D., and Clerbaux, C.: A unified approach to infrared aerosol remote sensing and type specification, Atmos. Chem. Phys., 13, 2195–2221, doi:10.5194/acp-13-2195-2013, 2013.

Clerbaux, C., Coheur, P.-F., Clarisse, L., Hadji-Lazaro, J., Hurtmans, D., Turquety, S., Bowman, K., Worden, H. and Carn, S. A., Measurements of SO2 profiles in volcanic plumes from the NASA Tropospheric Emission Spectrometer (TES), Geophys. Res. Lett., 35, L22807, doi:10.1029/2008GL035566, 2008.

Colette, A., Favez, O., Meleux, F., Chiappini, L., Haeffelin, M., Morille, Y., Malherbe, L., Papin, A., Bessagnet, B., Menut, L., Leoz, E., and Rouil, L.: Assessing in near real time the impact of the April 2010 Eyjafjallajökull ash plume on air quality, Atmos. Environ., 45, 1217–1221, doi:10.1016/j.atmosenv.2010.09.064, 2011.

Corradini, S., Merucci, L., and Prata, A. J.: Retrieval of SO_2 from thermal infrared satellite measurements: correction procedures for the effects of volcanic ash, Atmos. Meas. Tech., 2, 177–191, doi:10.5194/amt-2-177-2009, 2009.

Corradini, S., Merucci, L., Prata, A. J., and Piscini, A.: Volcanic ash and SO2 in the 2008 Kasatochi eruption: Retrievals comparison from different IR satellite sensors, J. Geophys. Res.-Atmos., 115, D00L21, doi:10.1029/2009JD013634, 2010.

Dahlback, A. and Stamnes, K.: A new spherical model for computing the radiation field available for photolysis and heating at twilight, Planet. Space Sci., 39, 671–683, doi:10.1016/0032-0633(91)90061-E, 1991.

Derimian, Y., Dubovik, O., Tanre, D., Goloub, P., Lapyonok, T., and Mortier, A.: Optical properties and radiative forcing of the Eyjafjallajökull volcanic ash layer observed over Lille, France, in 2010, J. Geophys. Res.-Atmos., 117, d00U25, doi:10.1029/2011JD016815, 2012.

Derrien, M. and Le Gléau, H.: MSG/SEVIRI cloud mask and type from SAFNWC, Int. J. Rem. Sens., 26, 4707–4732, doi:10.1080/01431160500166128, 2005.

Derrien, M. and Le Gléau, H.: Improvement of cloud detection near sunrise and sunset by temporal-differencing and region-growing techniques with real-time SEVIRI, Int. J. Rem. Sens., 31, 1765–1780, doi:10.1080/01431160902926632, 2010.

Di Biagio, C., di Sarra, A., and Meloni, D.: Large atmospheric shortwave radiative forcing by Mediterranean aerosols derived from simultaneous ground-based and spaceborne observations and dependence on the aerosol type and single scattering albedo, J. Geophys. Res.-Atmos., 115, D10209, doi:10.1029/2009JD012697, 2010.

Di Iorio, T., di Sarra, A., Sferlazzo, D. M., Cacciani, M., Meloni, D., Monteleone, F., Fuà, D., and Fiocco, G.: Seasonal evolution of the tropospheric aerosol vertical profile in the central Mediterranean and role of desert dust, J. Geophys. Res.-Atmos., 114, D02201, doi:10.1029/2008JD010593, 2009.

di Sarra, A., Pace, G., Meloni, D., De Silvestri, L., Piacentino, S., and Monteleone, F.: Surface short-wave radiative forcing of different aerosol types in the central Mediterranean, Geophys. Res. Lett., 35, L02714, doi:10.1029/2007GL032395, 2008.

di Sarra, A., Di Biagio, C., Meloni, D., Monteleone, F., Pace, G., Pugnaghi, S., and Sferlazzo, D.: Shortwave and longwave radiative effects of the intense Saharan dust event of 25-26 March 2010 at Lampedusa (Mediterranean Sea), J. Geophys. Res.-Atmos., 116, D23209, doi:10.1029/2011JD016238, 2011.

di Sarra, A., Sferlazzo, D., Meloni, D., Anello, F., Bommarito, C., Corradini, S., Silvestri, L. D., Iorio, T. D., Monteleone, F., Pace, G., Piacentino, S., and Pugnaghi, S.: Empirical correction of multifilter rotating shadowband radiometer (MFRSR) aerosol optical depths for the aerosol forward scattering and development of a long-term integrated MFRSR-Cimel dataset at Lampedusa, Appl. Optics, 54, 2725–2737, doi:10.1364/AO.54.002725, 2015.

Doeringer, D., Eldering, A., Boone, C. D., González Abad, G., and Bernath, P. F.: Observation of sulfate aerosols and SO2 from the Sarychev volcanic eruption using data from the Atmospheric Chemistry Experiment (ACE), J. Geophys. Res.-Atmos., 117, D03203, doi:10.1029/2011JD016556, 2012.

Dubovik, O. and King, M. D.: A flexible inversion algorithm for retrieval of aerosol optical properties from Sun and sky radiance measurements, J. Geophys. Res.-Atmos., 105, 20673–20696, doi:10.1029/2000JD900282, 2000.

Dubuisson, P., Giraud, V., Chomette, O., Chepfer, H., and Pelon, J.: Fast radiative transfer modeling for infrared imaging radiometry, J. Quant. Spectr. Radiat. T., 95, 201–220, doi:10.1016/j.jqsrt.2004.09.034, 2005.

Dubuisson, P., Herbin, H., Minvielle, F., Compiègne, M., Thieuleux, F., Parol, F., and Pelon, J.: Remote sensing of volcanic ash plumes from thermal infrared: a case study analysis from SEVIRI, MODIS and IASI instruments, Atmos. Meas. Tech., 7, 359–371, doi:10.5194/amt-7-359-2014, 2014.

Dulac, F.: Interactive comment on "Synergistic use of Lagrangian dispersion modelling, satellite and surface remote sensing measurements for the investigation of volcanic plumes: the Mount Etna eruption of 25-27 October 2013" by P. Sellitto et al., Atmos. Chem. Phys. Discuss., 15, C10614–C10620, 2015.

Flanner, M. G., Gardner, A. S., Eckhardt, S., Stohl, A., and Perket, J.: Aerosol radiative forcing from the 2010 Eyjafjallajökull volcanic eruptions, J. Geophys. Res.-Atmos., 119, 9481–9491, doi:10.1002/2014JD021977, 2014.

García, O. E., Díaz, J. P., Expósito, F. J., Díaz, A. M., Dubovik, O., Derimian, Y., Dubuisson, P., and Roger, J.-C.: Shortwave radiative forcing and efficiency of key aerosol types using AERONET data, Atmos. Chem. Phys., 12, 5129–5145, doi:10.5194/acp-12-5129-2012, 2012.

Gassó, S.: Satellite observations of the impact of weak volcanic activity on marine clouds, J. Geophys. Res.-Atmos., 113, D14S19, doi:10.1029/2007JD009106, 2008.

Georgoulias, A., Balis, D., Koukouli, M., Meleti, C., Bais, A., and Zerefos, C.: A study of the total atmospheric sulfur dioxide load using ground-based measurements and the satellite derived Sulfur Dioxide Index, Atmos. Environ., 43, 1693–1701, doi:10.1016/j.atmosenv.2008.12.012, 2009.

Gerlach, T.: Etna's greenhouse pump, Nature, 351, 352–353, doi:10.1038/351352a0, 1991.

Giammanco, S., Neri, M., Salerno, G. G., Caltabiano, T., Burton, M. R., and Longo, V.: Evidence for a recent change in the shallow plumbing system of Mt. Etna (Italy): Gas geochemistry and structural data during 2001–2005, J. Volcanol. Geoth. Res., 251, 90–97, doi:10.1016/j.jvolgeores.2012.06.001, 2013.

Graf, H.-F., Feichter, J., and Langmann, B.: Volcanic sulfur emissions: Estimates of source strength and its contribution to the global sulfate distribution, J. Geophys. Res., 102, 10727–10738, doi:10.1029/96JD03265, 1997.

Hamill, P., Jensen, E. J., Russell, P. B., and Bauman, J. J.: The Life Cycle of Stratospheric Aerosol Particles, B. Am. Meteorol. Soc., 78, 1395–1410, doi:10.1175/1520-0477(1997)078<1395:TLCOSA>2.0.CO;2, 1997.

Hobbs, P. V., Radke, L. F., Lyons, J. H., Ferek, R. J., Coffman, D. J., and Casadevall, T. J.: Airborne measurements of particle and gas emissions from the 1990 volcanic eruptions of Mount Redoubt, J. Geophys. Res.-Atmos., 96, 18735–18752, doi:10.1029/91JD01635, 1991.

Holben, B., Eck, T., Slutsker, I., Tanré, D., Buis, J., Setzer, A., Vermote, E., Reagan, J., Kaufman, Y., Nakajima, T., Lavenu, F., Jankowiak, I., and Smirnov, A.: AERONET – A Federated Instrument Network and Data Archive for Aerosol Characterization, Remote Sens. Environ., 66, 1–16, doi:10.1016/S0034-4257(98)00031-5, 1998.

Huebert, B. J., Phillips, C. A., Zhuang, L., Kjellström, E., Rodhe, H., Feichter, J., and Land, C.: Long-term measurements of free-tropospheric sulfate at Mauna Loa: Comparison with global model simulations, J. Geophys. Res.-Atmos., 106, 5479–5492, doi:10.1029/2000JD900627, 2001.

INGV: Bollettino settimanale sul monitoraggio vulcanico, geochimico e sismico del vulcano Etna, 21/10/2013–27/10/2013, Tech. Rep. 44/2013, Istituto Nazionale di Geofisica e Vulcanologia, 2013b.

INGV: L'attivitá parossistica del 26 ottobre 2013 al Nuovo Cratere di SE e al Cratere di NE: dispersione dei depositi di caduta e caratteristiche dei prodotti eruttati, INGV Open File Report, Rapporto UFVG del 2 novembre 2013, Tech. Rep. RPTVETCEN20131026, Istituto Nazionale di Geofisica e Vulcanologia, 2013a.

Karagulian, F., Clarisse, L., Clerbaux, C., Prata, A. J., Hurtmans, D. and Coheur P. F.: Detection of volcanic SO2, ash, and H2SO4 using the Infrared Atmospheric Sounding Interferometer (IASI), J. Geophys. Res., 115, D00L02, doi:10.1029/2009JD012786, 2010.

Kerr, J. B., McElroy, C. T., Wardle, D. I., Olafson, R. A., and Evans, W. F. J.: Atmospheric Ozone, chap. The automated Brewer spectrophotometer, p. 396–401, 1985.

Krotkov, N. A., Carn, S. A., Krueger, A. J., Bhartia, P. K., and Yang, K.: Band residual difference algorithm for retrieval of SO_2 from the Aura Ozone Monitoring Instrument (OMI), IEEE T. Geosci. Remote Sens., 44, 1259–1266, doi:10.1109/TGRS.2005.861932, 2006.

Kulmala, M., Kontkanen, J., Junninen, H., Lehtipalo, K., Manninen, H. E., Nieminen, T., Petäjä, T., Sipilä, M., Schobesberger, S., Rantala, P., Franchin, A., Jokinen, T., Järvinen, E., Äijälä, M., Kangasluoma, J., Hakala, J., Aalto, P. P., Paasonen, P., Mikkilä, J., Vanhanen, J., Aalto, J., Hakola, H., Makkonen, U., Ruuskanen, T., Mauldin, R. L., Duplissy, J., Vehkamäki, H., Bäck, J., Kortelainen, A., Riipinen, I., Kurtén, T., Johnston, M. V., Smith, J. N., Ehn, M., Mentel, T. F., Lehtinen, K. E. J., Laaksonen, A., Kerminen, V.-M., and Worsnop, D. R.: Direct Observations of Atmospheric Aerosol Nucleation, Science, 339, 943–946, doi:10.1126/science.1227385, 2013.

Kurucz, R.: Synthetic Infrared Spectra, in: Infrared Solar Physics, edited by: Rabin, D., Jefferies, J., and Lindsey, C., vol. 154 of International Astronomical Union/Union Astronomique Internationale, Springer, the Netherlands, 523–531, doi:10.1007/978-94-011-1926-9_62, 1994.

Mallet, M., Dulac, F., Formenti, P., Nabat, P., Sciare, J., Roberts, G., Pelon, J., Ancellet, G., Tanré, D., Parol, F., di Sarra, A., Alados, L., Arndt, J., Auriol, F., Blarel, L., Bourrianne, T., Brogniez, G., Chazette, P., Chevaillier, S., Claeys, M., D'Anna, B., Denjean, C., Derimian, Y., Desboeufs, K., Di Iorio, T., Doussin, J.-F., Durand, P., Féron, A., Freney, E., Gaimoz, C., Goloub, P., Gómez-Amo, J. L., Granados-Muñoz, M. J., Grand, N., Hamonou, E., Jankowiak, I., Jeannot, M., Léon, J.-F., Maillé, M., Mailler, S., Meloni, D., Menut, L., Momboisse, G., Nicolas, J., Podvin, J., Pont, V., Rea, G., Renard, J.-B., Roblou, L., Schepanski, K., Schwarzenboeck, A., Sellegri, K., Sicard, M., Solmon, F., Somot, S., Torres, B., Totems, J., Triquet, S., Verdier, N., Verwaerde, C., Wenger, J., and Zapf, P.: Overview of the Chemistry-Aerosol Mediterranean Experiment/Aerosol Direct Radiative Forcing on the Mediterranean Climate (ChArMEx/ADRIMED) summer 2013 campaign, Atmos. Chem. Phys., 16, 455–504, doi:10.5194/acp-16-455-2016, 2016.

Marconi, M., Sferlazzo, D. M., Becagli, S., Bommarito, C., Calzolai, G., Chiari, M., di Sarra, A., Ghedini, C., Gómez-Amo, J. L., Lucarelli, F., Meloni, D., Monteleone, F., Nava, S., Pace, G., Piacentino, S., Rugi, F., Severi, M., Traversi, R., and Udisti, R.: Saharan dust aerosol over the central

Mediterranean Sea: PM$_{10}$ chemical composition and concentration versus optical columnar measurements, Atmos. Chem. Phys., 14, 2039–2054, doi:10.5194/acp-14-2039-2014, 2014.

Martin, R. S., Mather, T. A., Pyle, D. M., Power, M., Allen, A. G., Aiuppa, A., Horwell, C. J., and Ward, E. P. W.: Composition-resolved size distributions of volcanic aerosols in the Mt. Etna plumes, J. Geophys. Res.-Atmos., 113, D17211, doi:10.1029/2007JD009648, 2008.

Mastin, L., Guffanti, M., Servranckx, R., Webley, P., Barsotti, S., Dean, K., Durant, A., Ewert, J., Neri, A., Rose, W., Schneider, D., Siebert, L., Stunder, B., Swanson, G., Tupper, A., Volentik, A., and Waythomas, C.: A multidisciplinary effort to assign realistic source parameters to models of volcanic ash-cloud transport and dispersion during eruptions, J. Volcanol. Geoth. Res., 186, 10–21, doi:10.1016/j.jvolgeores.2009.01.008, 2009.

Mather, T. A., Tsanev, V. I., Pyle, D. M., McGonigle, A. J. S., Oppenheimer, C., and Allen, A. G.: Characterization and evolution of tropospheric plumes from Lascar and Villarrica volcanoes, Chile, J. Geophys. Res.-Atmos., 109, D21303, doi:10.1029/2004JD004934, 2004.

Mayer, B. and Kylling, A.: Technical note: The libRadtran software package for radiative transfer calculations – description and examples of use, Atmos. Chem. Phys., 5, 1855–1877, doi:10.5194/acp-5-1855-2005, 2005.

McCormick, B. T., Herzog, M., Yang, J., Edmonds, M., Mather, T. A., Carn, S. A., Hidalgo, S., and Langmann, B.: A comparison of satellite- and ground-based measurements of SO$_2$ emissions from Tungurahua volcano, Ecuador, J. Geophys. Res.-Atmos., 119, 4264–4285, doi:10.1002/2013JD019771, 2014.

McCormick, M. P., Thomason, L. W., and Trepte, C. R.: Atmospheric effects of the Mt Pinatubo eruption, Nature, 373, 399–404, doi:10.1038/373399a0, 1995.

McGonigle, A. J. S., Delmelle, P., Oppenheimer, C., Tsanev, V. I., Delfosse, T., Williams-Jones, G., Horton, K., and Mather, T. A.: SO$_2$ depletion in tropospheric volcanic plumes, Geophys. Res. Lett., 31, L13201, doi:10.1029/2004GL019990, 2004.

Meloni, D., di Sarra, A., DeLuisi, J., Iorio, T. D., Fiocco, G., Junkermann, W., and Pace, G.: Tropospheric Aerosols in the Mediterranean: 2. Radiative effects through model simulations and measurements, J. Geophys. Res., 108, 4317, doi:10.1029/2002JD002807, 2003.

Meloni, D., di Sarra, A., Herman, J. R., Monteleone, F., and Piacentino, S.: Comparison of ground-based and Total Ozone Mapping Spectrometer erythemal UV doses at the island of Lampedusa in the period 1998-2003: Role of tropospheric aerosols, J. Geophys. Res.-Atmos., 110, D01202, doi:10.1029/2004JD005283, 2005a.

Meloni, D., di Sarra, A., Iorio, T. D., and Fiocco, G.: Influence of the vertical profile of Saharan dust on the visible direct radiative forcing, J. Quant. Spectr. Radiat. T., 93, 397–413, doi:10.1016/j.jqsrt.2004.08.035, 2005b.

Meloni, D., di Sarra, A., Biavati, G., DeLuisi, J., Monteleone, F., Pace, G., Piacentino, S., and Sferlazzo, D.: Seasonal behavior of Saharan dust events at the Mediterranean island of Lampedusa in the period 1999–2005, Atmos. Environ., 41, 3041–3056, doi:10.1016/j.atmosenv.2006.12.001, 2007.

Merucci, L., Burton, M., Corradini, S., and Salerno, G. G.: Reconstruction of SO_2 flux emission chronology from space-based measurements, J. Volcanol. Geoth. Res., 206, 80–87, doi:10.1016/j.jvolgeores.2011.07.002, 2011.

O'Neill, N. T., Eck, T. F., Smirnov, A., Holben, B. N., and Thulasiraman, S.: Spectral discrimination of coarse and fine mode optical depth, J. Geophys. Res.-Atmos., 108, 4559, doi:10.1029/2002JD002975, 2003.

Oppenheimer, C., Francis, P., and Stix, J.: Depletion rates of sulfur dioxide in tropospheric volcanic plumes, Geophys. Res. Lett., 25, 2671–2674, doi:10.1029/98GL01988, 1998.

Oppenheimer, C., Scaillet, B., and Martin, R. S.: Sulfur Degassing From Volcanoes: Source Conditions, Surveillance, Plume Chemistry and Earth System Impacts, Rev. Mineral. Geochem., 72, 363–421, doi:10.2138/rmg.2011.73.13, 2011.

Patanè, D., Aiuppa, A., Aloisi, M., Behncke, B., Cannata, A., Coltelli, M., Di Grazia, G., Gambino, S., Gurrieri, S., Mattia, M., and Salerno, G.: Insights into magma and fluid transfer at Mount Etna by a multiparametric approach: A model of the events leading to the 2011 eruptive cycle, J. Geophys. Res.-Solid Earth, 118, 3519–3539, doi:10.1002/jgrb.50248, 2013.

Pierluissi, J. H. and Peng, G.-S.: New Molecular Transmission Band Models For LOWTRAN, Optical Eng., 24, 243541–243541, doi:10.1117/12.7973523, 1985.

Prata, A. J. and Grant, I. F.: Retrieval of microphysical and morphological properties of volcanic ash plumes from satellite data: Application to Mt Ruapehu, New Zealand, Q. J. Roy. Meteorol. Soc., 127, 2153–2179, doi:10.1002/qj.49712757615, 2001.

Pugnaghi, S., Gangale, G., Corradini, S., and Buongiorno, M.: Mt. Etna sulfur dioxide flux monitoring using ASTER-TIR data and atmospheric observations, J. Volcanol. Geoth. Res., 152, 74–90, doi:10.1016/j.jvolgeores.2005.10.004, 2006.

Pugnaghi, S., Guerrieri, L., Corradini, S., Merucci, L., and Arvani, B.: A new simplified approach for simultaneous retrieval of SO_2 and ash content of tropospheric volcanic clouds: an application to the Mt Etna volcano, Atmos. Meas. Tech., 6, 1315–1327, doi:10.5194/amt-6-1315-2013, 2013.

Ricchiazzi, P., Yang, S., Gautier, C., and Sowle, D.: SBDART: a research and teaching software tool for plane-parallel radiative transfer in the earth's atmosphere, B. Am. Meteorol. Soc., 79, 2101–2114, doi:10.1175/1520-0477(1998)079<2101:SARATS>2.0.CO;2, 1998.

Ridley, D. A., Solomon, S., Barnes, J. E., Burlakov, V. D., Deshler, T., Dolgii, S. I., Herber, A. B., Nagai, T., Neely, R. R., Nevzorov, A. V., Ritter, C., Sakai, T., Santer, B. D., Sato, M., Schmidt, A., Uchino, O., and Vernier, J. P.: Total volcanic stratospheric aerosol optical depths and implications for global climate change, Geophys. Res. Lett., 41(22), 7763–7769, doi:10.1002/2014GL061541, 2014.

Robock, A. and Oppenheimer, C.: Volcanism and the Earth's Atmosphere, vol. 139 of Geophysical Monograph Series, American Geophysical Union, 2003.

Rothman, L., Gordon, I., Babikov, Y., Barbe, A., Benner, D. C., Bernath, P., Birk, M., Bizzocchi, L., Boudon, V., Brown, L., Campargue, A., Chance, K., Cohen, E., Coudert, L., Devi, V., Drouin, B., Fayt, A., Flaud, J.-M., Gamache, R., Harrison, J., Hartmann, J.-M., Hill, C., Hodges, J., Jacquemart, D., Jolly, A., Lamouroux, J., Roy, R. L., Li, G., Long, D., Lyulin, O., Mackie, C., Massie, S., Mikhailenko, S., Mueller, H. S. P., Naumenko, O., Nikitin, A., Orphal, J., Perevalov, V., Perrin, A., Polovtseva, E., Richard, C., Smith, M., Starikova, E., Sung, K., Tashkun, S., Tennyson, J., Toon, G., Tyuterev, V., and Wagner, G.: The HITRAN2012 molecular spectroscopic database, J. Quant. Spectr. Radiat. T., 130, 4–50, doi:10.1016/j.jqsrt.2013.07.002, 2013.

Salerno, G., Burton, M., Oppenheimer, C., Caltabiano, T., Randazzo, D., Bruno, N., and Longo, V.: Three-years of {SO2} flux measurements of Mt. Etna using an automated {UV} scanner array: Comparison with conventional traverses and uncertainties in flux retrieval, J. Volcanol. Geoth. Res., 183, 76–83, doi:10.1016/j.jvolgeores.2009.02.013, 2009a.

Salerno, G., Burton, M., Oppenheimer, C., Caltabiano, T., Tsanev, V., and Bruno, N.: Novel retrieval of volcanic {SO2} abundance from ultraviolet spectra, J. Volcanol. Geoth. Res., 181, 141–153, doi:10.1016/j.jvolgeores.2009.01.009, 2009b.

Santer, B. D., Bonfils, C., Painter, J. F., Zelinka, M. D., Mears, C., Solomon, S., Schmidt, G. A., Fyfe, J. C., Cole, J. N. S., Nazarenko, L., Taylor, K. E., and Wentz, F. J.: Volcanic contribution to decadal changes in tropospheric temperature, Nature Geosci., 7, 185–189, doi:10.1038/ngeo2098, 2014.

Satsumabayashi, H., Kawamura, M., Katsuno, T., Futaki, K., Murano, K., Carmichael, G. R., Kajino, M., Horiguchi, M., and Ueda, H.: Effects of Miyake volcanic effluents on airborne particles and precipitation in central Japan, J. Geophys. Res.-Atmos., 109, D19202, doi:10.1029/2003JD004204, 2004.

Schmetz, J., Holmlund, K., Hoffman, J., Strauss, B., Mason, B., Gaertner, V., Koch, A., and Van De Berg, L.: Operational Cloud-Motion Winds from Meteosat Infrared Images, J. Appl. Meteorol., 1206–1225, doi:10.1175/1520-0450(1993)032<1206:OCMWFM>2.0.CO;2, 1993.

Schmidt, G. A., Shindell, D. T., and Tsigaridis, K.: Reconciling warming trends, Nature Geosci., 7, 158–160, doi:10.1038/ngeo2105, 2014.

Sellitto, P. and Briole, P.: On the radiative forcing of volcanic plumes: modelling the impact of Mount Etna in the Mediterranean, Annals of Geophysics, 58, ISSN 2037–416X, 2015.

Sellitto, P. and Legras, B.: Sensitivity of thermal infrared sounders to the chemical and microphysical properties of UTLS secondary sulphate aerosols, Atmos. Meas. Tech., 9, 115–132, doi:10.5194/amt-9-115-2016, 2016.

Sellitto, P., Zanetel, C., di Sarra, A., Salerno, G., Tapparo, A., Briole, P., and Legras, B. The impact of Mount Etna's sulphur emissions to the atmospheric composition, aerosol properties and radiative transfer in the central Mediterranean: 14 years of statistic analysis using observations and Lagrangian modelling, Geophysical Research Abstracts, 18, EGU2016-16001-1, 2016.

Sèze, G., Pelon, J., Derrien, M., Le Gléau, H., and Six, B.: Evaluation against CALIPSO lidar observations of the multi-geostationary cloud cover and type dataset assembled in the framework of the Megha-Tropiques mission, Q. J. Roy. Meteorol. Soc., 774–797, doi:10.1002/qj.2392, 2014.

Shettle, E.: Models of aerosols, clouds and precipitation for atmospheric propagation studies, in: Atmospheric propagation in the uv, visible, ir and mm-region and related system aspects, no. 454 AGAD Conference Proceedings, 1989.

SPARC: Assessment of Stratospheric Aerosol Properties, Tech. Rep. 4, Stratosphere-Troposphere Processes and their Role on Climate, 2006.

Stephens, G.: Remote Sensing of the Lower Atmosphere: An Introduction, Oxford University Press, http://books.google.fr/books?id=3FkRAQAAIAAJ (last access: 5 November 2015), 1994.

Stevenson, D. S., Johnson, C. E., Collins, W. J., and Derwent, R. G.: The tropospheric sulphur cycle and the role of volcanic SO2, Geological Society, London, Special Publications, 213, 295–305, doi:10.1144/GSL.SP.2003.213.01.18, 2003.

Stohl, A., Forster, C., Frank, A., Seibert, P., and Wotawa, G.: Technical note: The Lagrangian particle dispersion model FLEXPART version 6.2, Atmos. Chem. Phys., 5, 2461–2474, doi:10.5194/acp-5-2461-2005, 2005.

Stohl, A., Prata, A. J., Eckhardt, S., Clarisse, L., Durant, A., Henne, S., Kristiansen, N. I., Minikin, A., Schumann, U., Seibert, P., Stebel, K., Thomas, H. E., Thorsteinsson, T., Tørseth, K., and Weinzierl, B.: Determination of time- and height-resolved volcanic ash emissions and their use for

quantitative ash dispersion modeling: the 2010 Eyjafjallajökull eruption, Atmos. Chem. Phys., 11, 4333–4351, doi:10.5194/acp-11-4333-2011, 2011.

Theys, N., Campion, R., Clarisse, L., Brenot, H., van Gent, J., Dils, B., Corradini, S., Merucci, L., Coheur, P.-F., Van Roozendael, M., Hurtmans, D., Clerbaux, C., Tait, S., and Ferrucci, F.: Volcanic SO$_2$ fluxes derived from satellite data: a survey using OMI, GOME-2, IASI and MODIS, Atmos. Chem. Phys., 13, 5945–5968, doi:10.5194/acp-13-5945-2013, 2013.

Vehkamäki, H., Kulmala, M., Napari, I., Lehtinen, K. E. J., Timmreck, C., Noppel, M., and Laaksonen, A.: An improved parameterization for sulfuric acid-water nucleation rates for tropospheric and stratospheric conditions, J. Geophys. Res.-Atmos., 107, AAC 3-1–AAC 3-10, doi:10.1029/2002JD002184, 2002.

von Glasow, R., Bobrowski, N., and Kern, C.: The effects of volcanic eruptions on atmospheric chemistry, Chem. Geology, 263, 131–142, doi:10.1016/j.chemgeo.2008.08.020, 2009.

Waquet, F., Peers, F., Goloub, P., Ducos, F., Thieuleux, F., Derimian, Y., Riedi, J., Chami, M., and Tanré, D.: Retrieval of the Eyjafjallajökull volcanic aerosol optical and microphysical properties from POLDER/PARASOL measurements, Atmos. Chem. Phys., 14, 1755–1768, doi:10.5194/acp-14-1755-2014, 2014.

Watson, I. M. and Oppenheimer, C.: Particle size distributions of Mount Etna's aerosol plume constrained by Sun photometry, J. Geophys. Res.-Atmos., 105, 9823–9829, doi:10.1029/2000JD900042, 2000.

Watson, I. M. and Oppenheimer, C.: Photometric observations of Mt. Etna's different aerosol plumes, Atmos. Environ., 35, 3561–3572, doi:10.1016/S1352-2310(01)00075-9, 2001.

Webley, P. W., Steensen, T., Stuefer, M., Grell, G., Freitas, S., and Pavolonis, M.: Analyzing the Eyjafjallajökull 2010 eruption using satellite remote sensing, lidar and WRF-Chem dispersion and tracking model, J. Geophys. Res.-Atmos., 117, D00U26, doi:10.1029/2011JD016817, 2012.

Zhuang, B. L., Wang, T.J. , Li, S., Liu, J., Talbot, R., Mao, H.T., Yang, X.Q., Fu, C.B., Yin, C.Q., Zhu, J.L., Che, H.Z., and Zhang, X.Y.: Optical properties and radiative forcing of urban aerosols in Nanjing, China, Atmospheric Environment, 83, 43–52, doi:http://dx.doi.org/10.1016/j.atmosenv.2013.10.052, 2014.

Table 1. Size distribution of the ash particles in the FLEXPART simulations.

Radius (μm)	Mass fraction (%)
0.1	1
0.35	2
1.0	5
3.5	20
10.0	60
32.5	12

Table 2. Top of the atmosphere (TOA) and surface daily radiative forcing efficiency (RFE), and the ratio f=surface daily RFE/TOA daily RFE, as a function of the single scattering albedo (SSA).

SSA	TOA daily RFE (W m^{-2} AOD^{-1})	Surface daily RFE (W m^{-2} AOD^{-1})	f
0.92	-38.9	-65.7	1.7
0.97	-44.7	-54.3	1.2
0.98	-46.2	-51.4	1.1
0.99	-47.7	-48.6	1.0

Table 3. TOA and surface daily RFE, and the ratio f, as a function of the surface albedo.

Surface albedo	TOA daily RFE (W m^{-2} AOD^{-1})	Surface daily RFE (W m^{-2} AOD^{-1})	f
0.07 (sea)	-46.4	-51.0	1.0
0.09 (Lampedusa)	-46.2	-51.4	1.1
0.36 (desert)	-13.9	-27.1	1.9
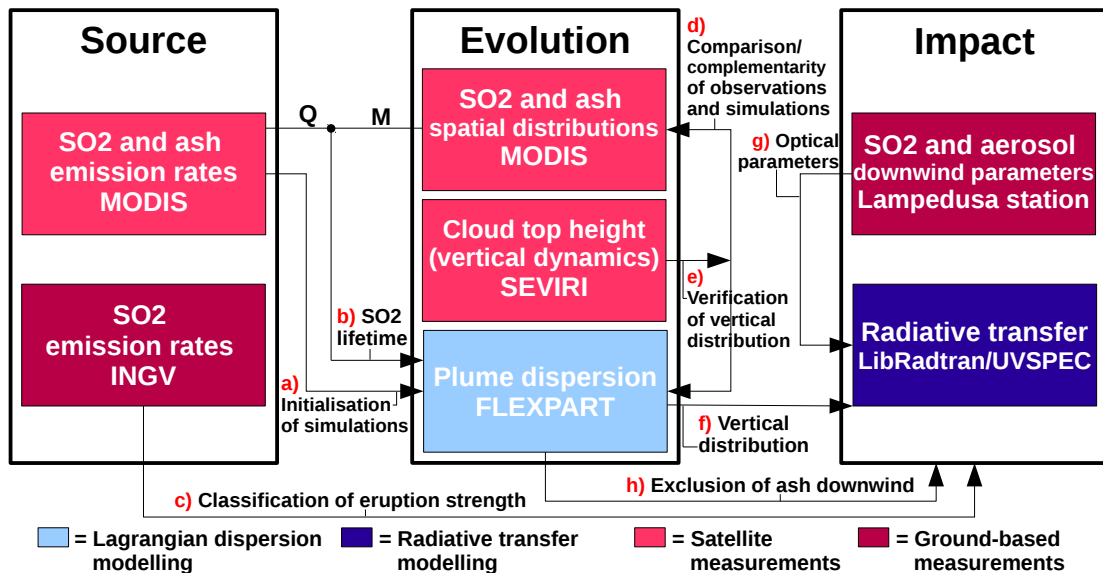
Figure 1. Scheme of the synergies of the different methods described in Sects. 2.2.1 - 2.3.2. From a) to h) the different synergies and contributions of the methods are indicated as they are referenced throughout the text. The symbols M and Q refer to the SO_2 mass loading and the SO2 emission rate of Eq. 1.
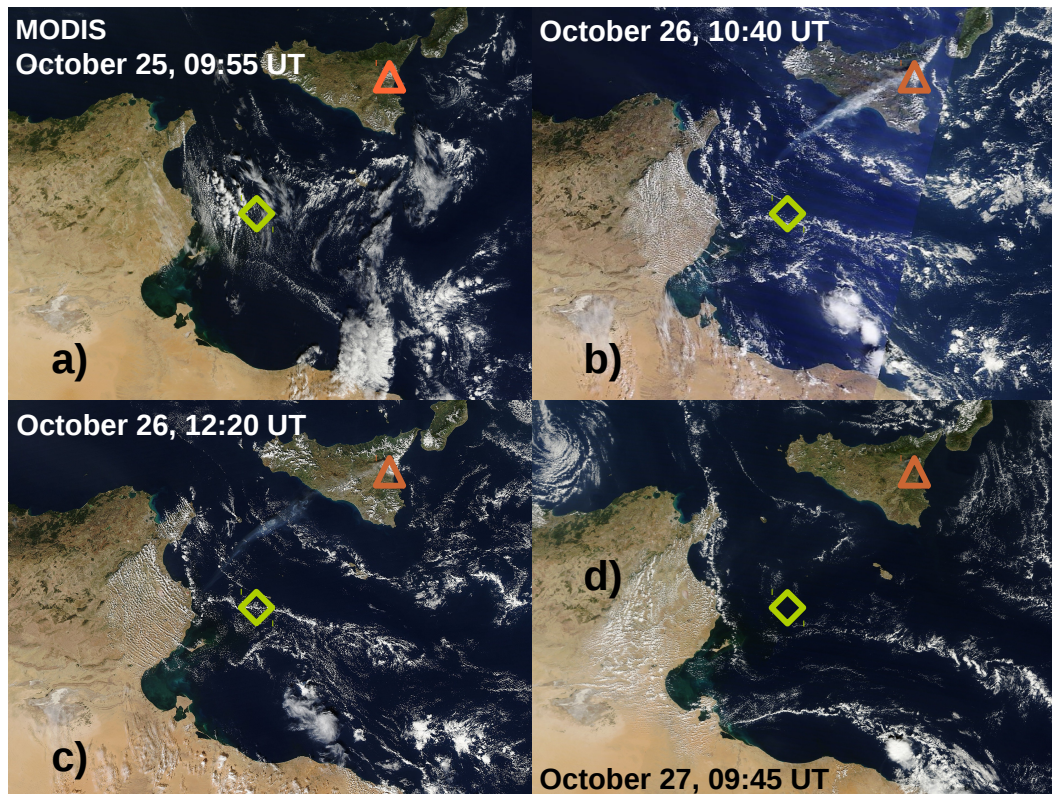
Figure 2. (a-d) MODIS true color images showing the Mount Etna plume evolution during the period 25–27 October 2013. The position of Mount Etna is indicated with an orange triangle. The position of Lampedusa is indicated with a light green diamond.
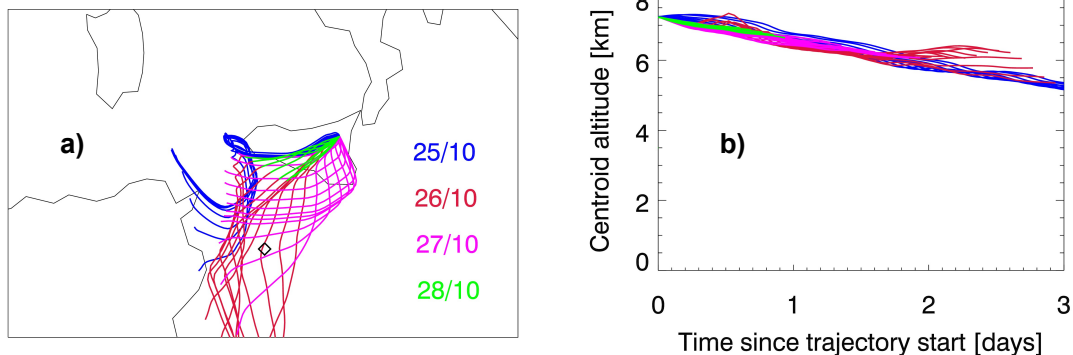
Figure 3. (a) Bi-hourly forward trajectories of the volcanic plume, taken as the centroid of the sulphur dioxide plume, for the period 25–28 October 2013, from FLEXPART simulations. Each trajectory has temporal duration of about 3 days. Different days are identified with different colors. The position of Lampedusa is indicated with a black diamond. **(b)** Average altitude of the plumes for each trajectory identified in plot **(a)**, taken as the centroid of the sulphur dioxide plume, from FLEXPART simulations.
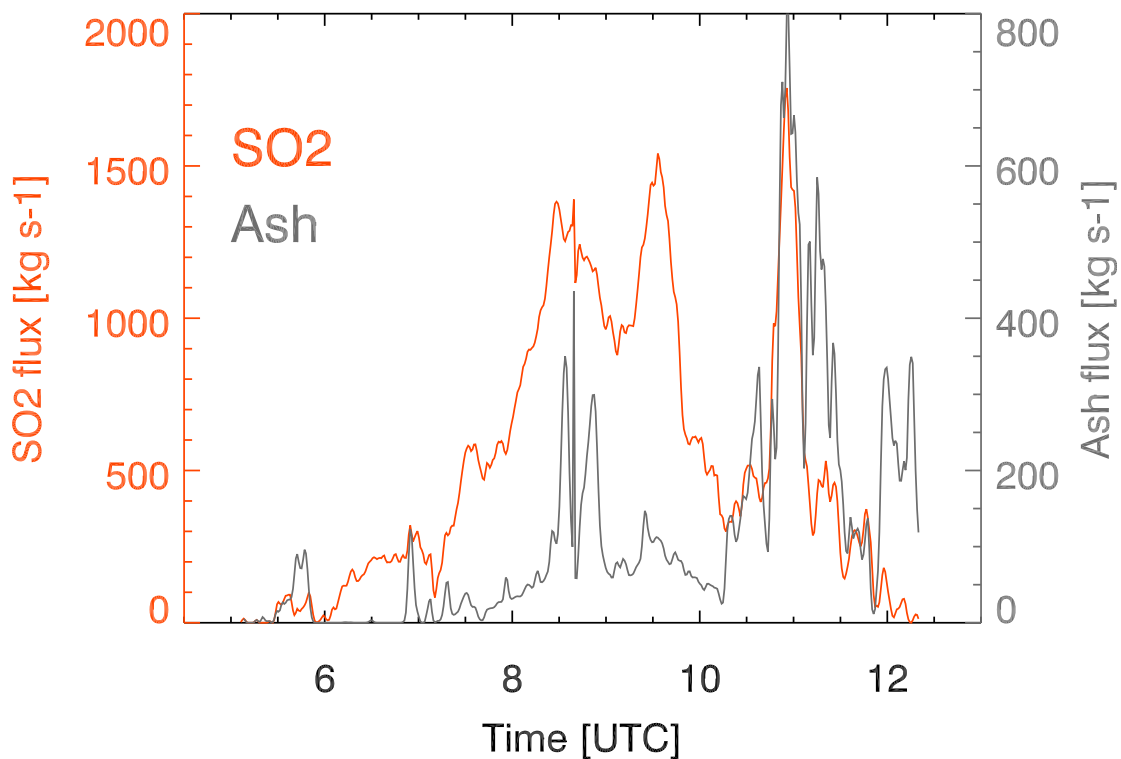
Figure 4. Sulphur dioxide (orange) and ash (gray) emissions (in $kg\,s^{-1}$) for 26 October 2013, estimated with the Aqua-MODIS inverse method.
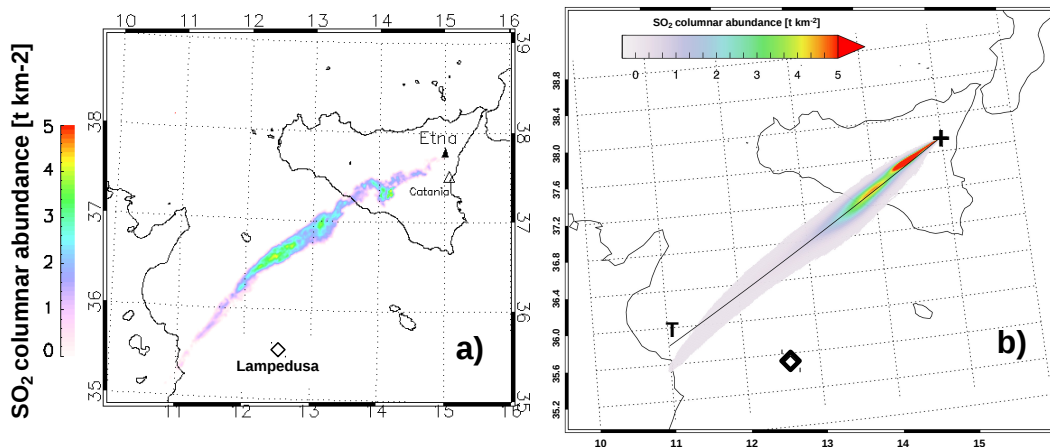
Figure 5. (a) Sulphur dioxide column abundance (in $t\,km^{-2}$ – tons per square km) derived from Aqua-MODIS overpass of 26 October 2013, 12:20. The position of Lampedusa is indicated with a black diamond; **(b)** sulphur dioxide column abundance (in $t\,km^{-2}$) from FLEXPART simulations, for 26 October 2013, 12:20. Violet-grey to red pixels indicate relatively low to high abundance values. The position of Lampedusa is indicated with a black diamond; the position of Mount Etna is indicated with a black cross; the trajectory T is representative of the plume axis.
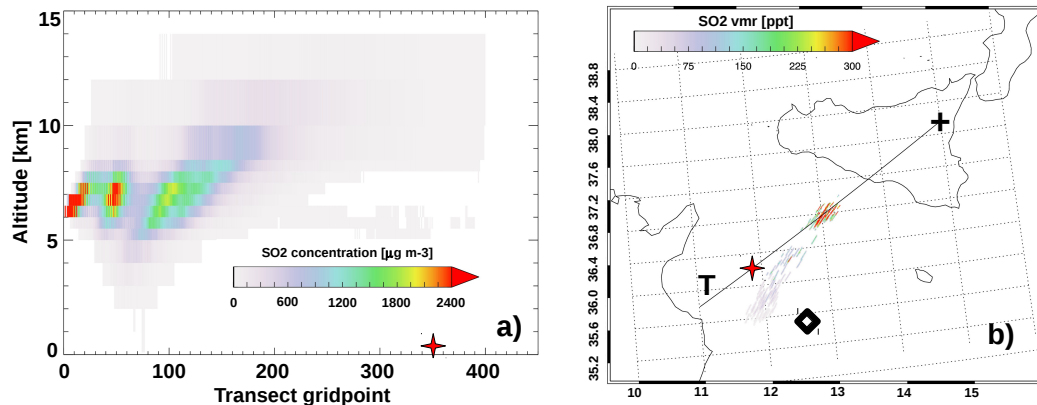
Figure 6. (a) Sulphur dioxide vertical concentration profiles (in µg m^{-3}) along trajectory *T* and **(b)** the mean volume mixing ratio (in ppt – part per trillion) in the altitude range from 10 to 14 km, from FLEXPART simulations, for 26 October 2013, 12:20. Violet-grey to red pixels indicate relatively low to high concentration values. The red cross marks the same gridpoints in **(a)** and **(b)**. The position of Lampedusa is indicated with a black diamond; the position of Mount Etna is indicated with a black cross in **(b)**.
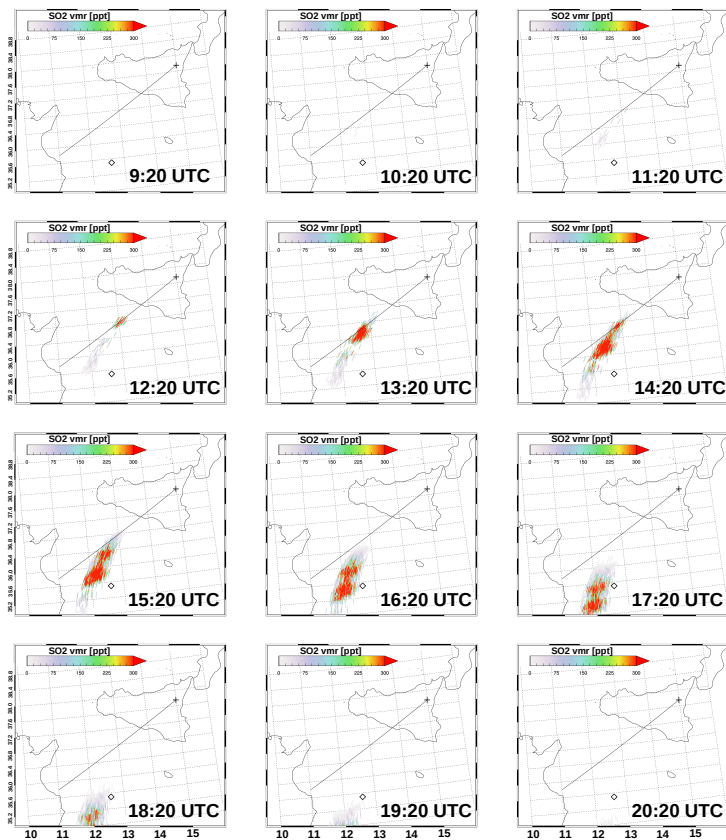
Figure 7. Mean SO_2 volume mixing ratio (in ppt) in the altitude range from 10 to 14 km, from FLEX-PART simulations, for 26 October 2013 from 09:20 to 20:20 (1 h time step, times indicated in the figure panel). Violet-grey to red pixels indicate relatively low to high mixing ratio values. The position of Lampedusa is indicated with a black diamond; the position of Mount Etna is indicated with a black cross.
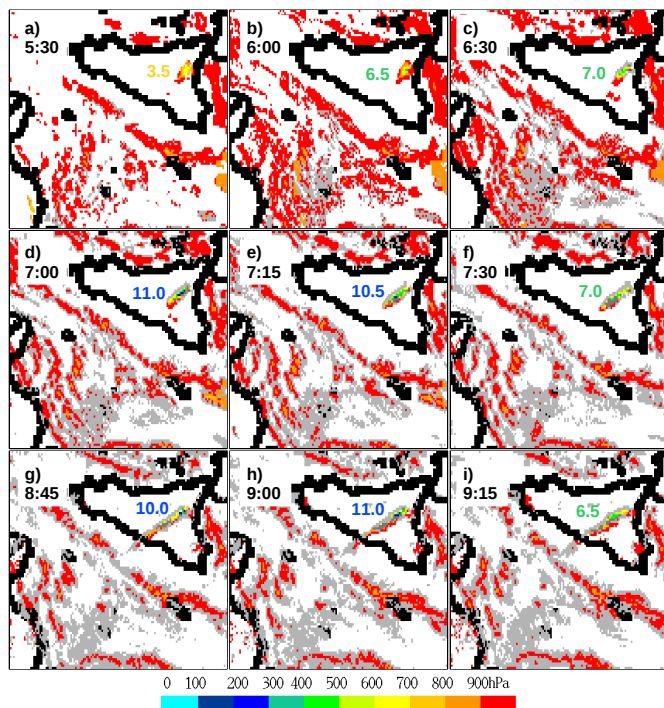
Figure 8. Cloud top pressure (in hPa) from SEVIRI, for 26 October 2013. Blue and red pixels indicate relatively low and high pressure values. The start time of the SEVIRI scan is reported at the top/left corner of each image. The cloud top altitude is obtained by comparing pressure and altitude profiles using a quasi-coincident radio-sounding at the WMO station in Trapani, Sicily, Italy (37.92° N, 12.50° E, 7 m above sea level), and is reported (in km) and color coded in the images. Partially cloud covered pixels and very thin clouds, for which no pressure is available, are respectively in light grey and grey.
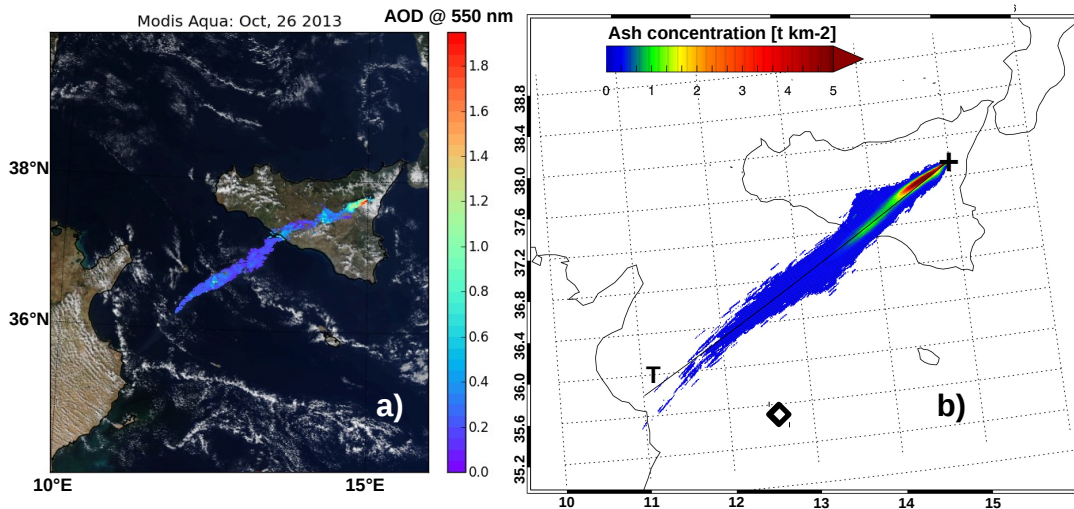
Figure 9. (a) Ash optical depth at 550 nm from Aqua-MODIS overpass of 26 October 2013, 12:20; **(b)** total ash column abundance (in t km^{-2}) from FLEXPART simulations. The ash classes 3, 4 and 5 (see Table 1) are added up to compare with MODIS observations. Blue to red pixels indicate relatively low to high optical depth (panel **(a)**) and abundance values (panel **(b)**). The position of Lampedusa is indicated with a black diamond in **(b)**; the position of Mount Etna is indicated with a black cross in **(b)**.
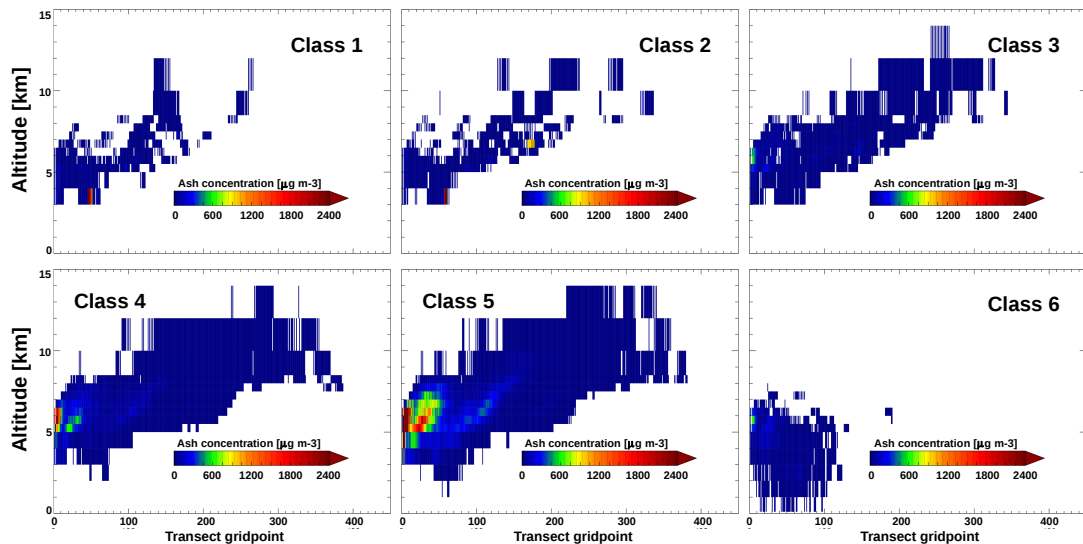
Figure 10. Ash vertical concentration profiles (in $\mu g\,m^{-3}$) for the 6 aerosol classes listed in Table 1, and identified in each panel, along the trajectory *T* of Figs. 5, 6, 7 and 9. Blue to red points indicate relatively low to high concentration values.
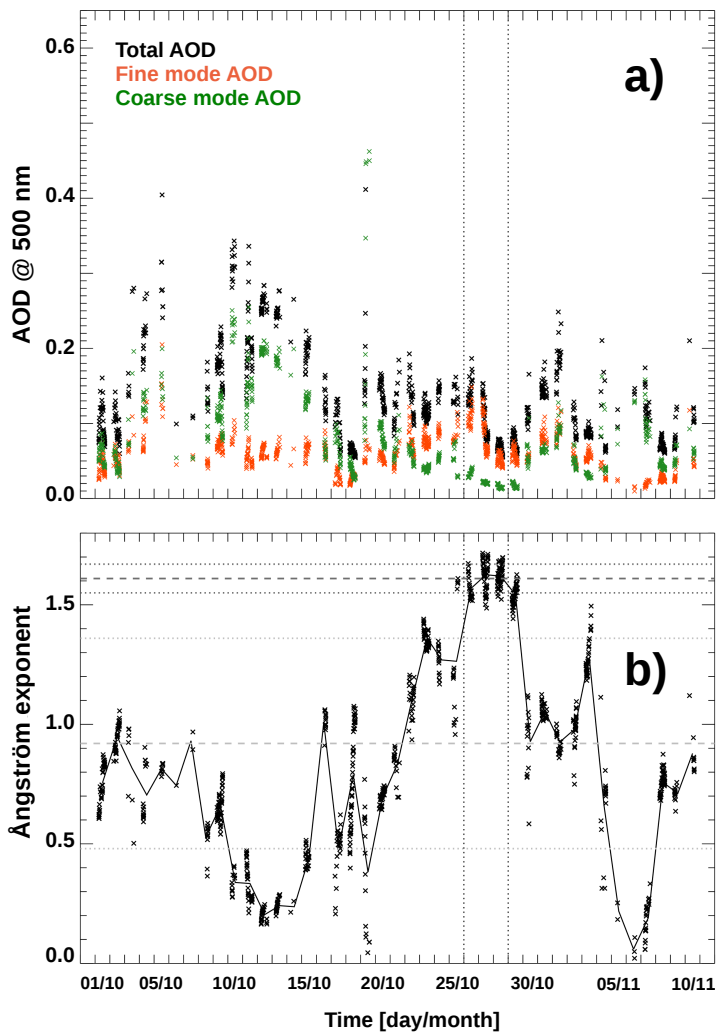
Figure 11. (a) Total (black crosses), fine mode (orange crosses) and coarse mode (green crosses) aerosol optical depth measurements; **(b)** Ångström exponent measurements (black crosses) and daily means (black line) at Lampedusa for the period 1 October to 10 November 2013. The vertical lines indicate the period 26–29 October 2013. The average for the period 26–29 October (black dashed horizontal line), plus and minus one standard deviation (black dotted horizontal lines), as well as the average for the whole month of October 2013 (gray dashed horizontal line), plus and minus one standard deviation (gray dotted horizontal lines) are also reported for the Ångström exponent.
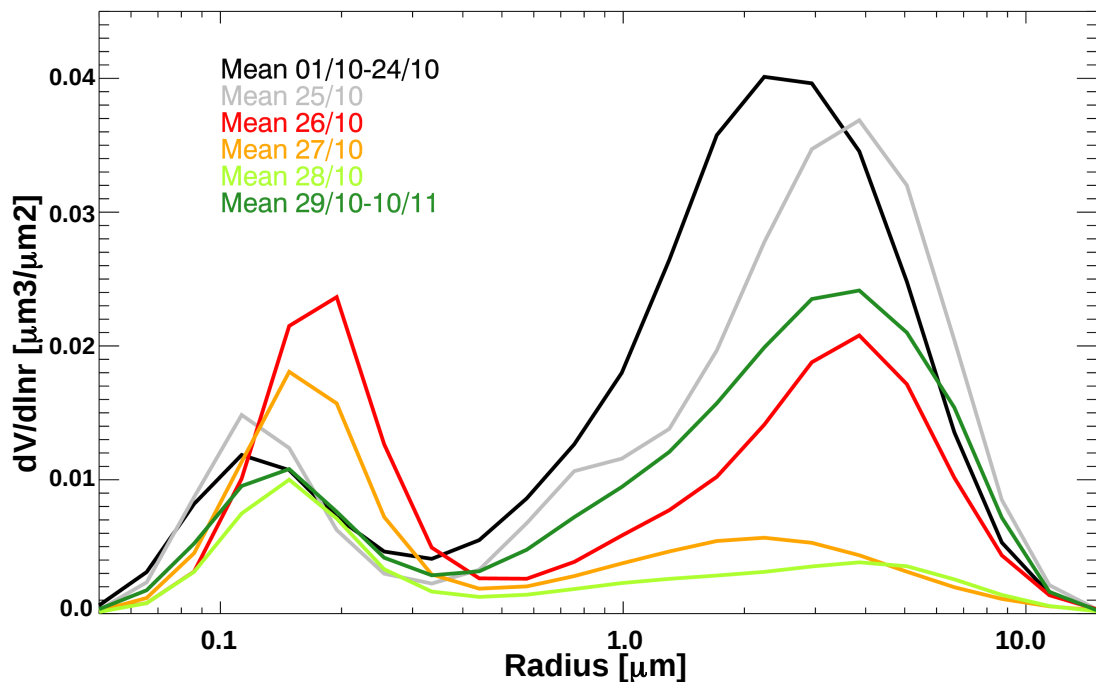
Figure 12. Aerosol size distributions (volume distribution, in µg^3 µg^{-2}) at Lampedusa for some selected periods before, during and after Mount Etna's eruption of 25–28 October 2013. The average from 1 to 24 October (black line), 25 (gray line), 26 (red line), 27 (orange line), 28 (light green line), 29 October to 10 November (dark green line) are shown.